2-

X-621-72-90

PREPRINT

NASA TM X- 65923

ROLE OF GAS SURFACE INTERACTIONS IN THE REDUCTION OF OGO-6 NEUTRAL GAS PARTICLE MASS SPECTROMETER DATA

A. E. HEDIN
B. B. HINTON
G. A. SCHMITT

MARCH 1972

GSFC — GODDARD SPACE FLIGHT CENTER
GREENBELT, MARYLAND

X-621-72-90

ROLE OF GAS-SURFACE INTERACTION IN THE REDUCTION OF OGO-6 NEUTRAL PARTICLE MASS SPECTROMETER DATA

A. E. Hedin
Goddard Space Flight Center
Greenbelt, Maryland

and

B. B. Hinton and G. A. Schmitt
Space Physics Research Laboratory
University of Michigan
Ann Arbor, Michigan

March 1972

Goddard Space Flight Center
Greenbelt, Maryland

CONTENTS

ROLE OF GAS-SURFACE INTERACTIONS IN THE REDUCTION OF OGO-6 NEUTRAL PARTICLE MASS SPECTROMETER DATA

INTRODUCTION

Several authors have pointed out that gas-surface interactions complicate the interpretation of neutral density measurements in the thermosphere (von Zahn, 1967; Moe and Moe, 1967, 1969; Silverman and Newton, 1970). This paper describes the gas-surface interaction effects observed by the OGO-6 neutral particle mass spectrometer and summarizes the technique developed to account for them in determining ambient neutral densities.

DESCRIPTION OF THE EXPERIMENT

OGO-6 is a polar-orbiting geophysical observatory (inclination 82° prograde) with an apogee of approximately 1100 km and perigee of about 400 km. The neutral particle mass spectrometer is mounted in an orbital plane experiment package (OPEP) such that in the normal mode of operation, the spectrometer inlet faces the spacecraft's direction of travel. In this mode, the flux of ambient neutral molecules entering the spectrometer is modulated primarily by the varying ambient density as the spacecraft changes altitude and position. On command, the OPEP can be rotated cyclically through 220° about a vertical axis, effecting an angle-of-attack modulation of the incoming flux of ambient molecules.

The quadrupole mass spectrometer employs an electron-impact ion source behind a gold-plated stainless steel antechamber (Figure 1). Ambient neutral molecules enter the antechamber through a knife-edged orifice and undergo many surface collisions before entering the ion source region. Ions created by impact with a beam of 75 V electrons in the source region are focused by an electrostatic lens and filtered according to their charge-to-mass ratios. Details of the instrument construction and operation have been documented elsewhere (Carignan and Pinkus, 1968).

In the normal mode, the total ion current and the ion currents for ions with molecular weights 2, 4, 16, 28, and 32 are sampled for 1.152 sec once every 9.216 sec, for 258 sec out of a 368 sec cycle. During 110 sec of the 368 sec cycle the spectrometer is in sweep mode, during which each ion in the range 1-46 amu is sampled at least twice. A continuous sweep mode is available on command, and masses of 2, 4, 28, 32 or total can be sampled continuously on command.

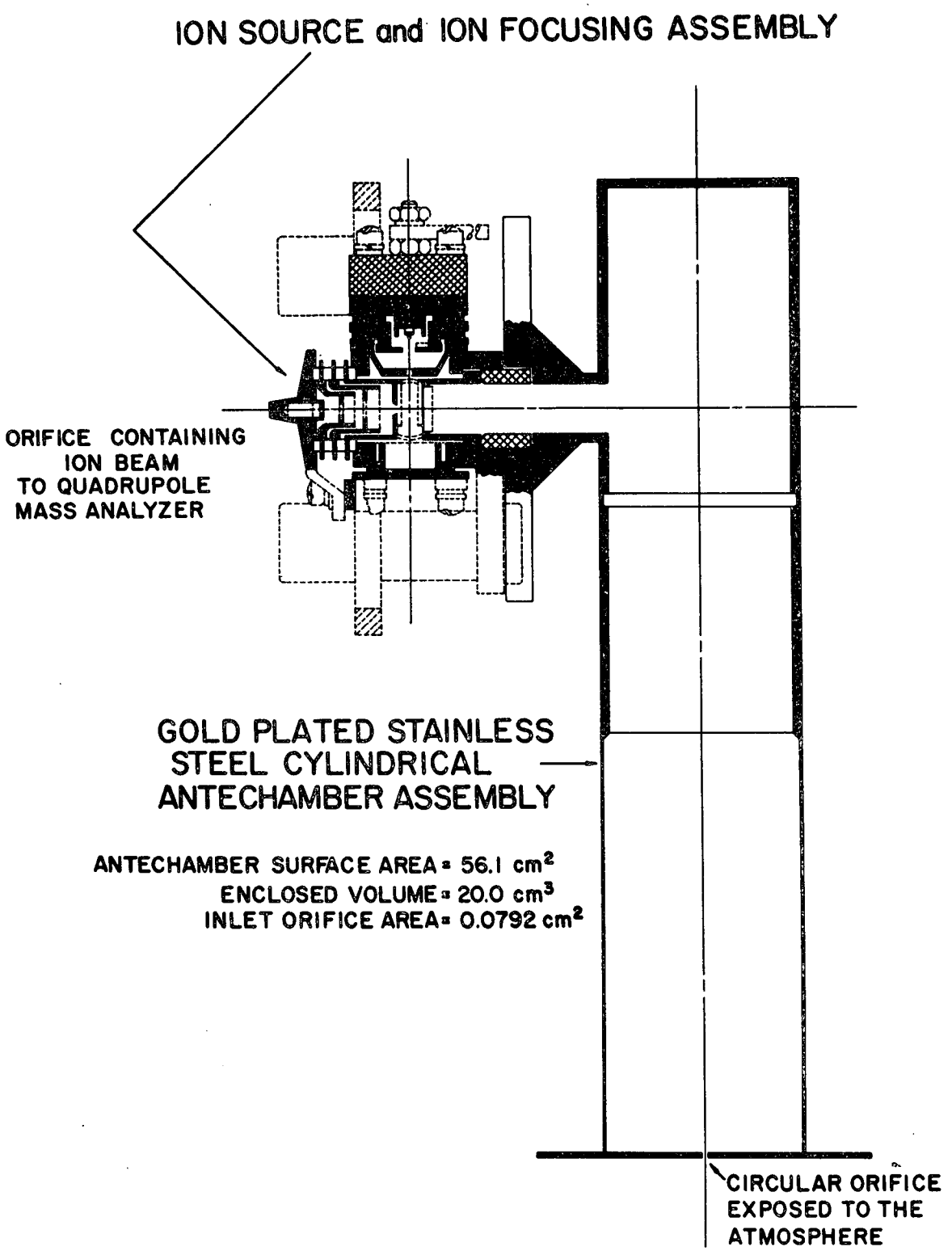

Figure 1. Cross section of the mass spectrometer antechamber and ion source. The antechamber is a cylinder with an inlet aperture on its axis.

GENERAL OBSERVATIONS

Assuming the incoming ambient molecules are thermally accommodated to the antechamber surface temperature, we can write the following equation for the number density of any constituent in the ion source region:

$$\frac{d n_g}{d t} = \left(\frac{1}{4} n_a F(s) \bar{c}_a A_h - \frac{1}{4} n_g \bar{c} A_h \right) \Big/ V \qquad (1)$$

$$F(s) = 2 \pi^{1/2} V_n / \bar{c}_a \quad \text{for} \quad V_n >> \bar{c}_a \qquad (2)$$

where

V_n is the spacecraft velocity component normal to the inlet orifice

n_g is the ion source number density

n_a is the ambient number density

A_h is the area of the inlet knife-edged orifice

$\bar{c}$ is the mean thermal speed of the constituent molecules at the surface temperature

$\bar{c}_a$ is the mean thermal speed of the constituent molecules in the ambient gas

V is the volume enclosed by the gauge

$F(s)$ is the thermal transpiration equation for a closed ion source, given in Equation (2) above.

Equation (1) describes the balance of molecular fluxes into and out of the spectrometer and may be used to consider the response of the source density to changes in incoming flux. For example, if the incoming flux went to zero, then

$$\frac{d n_g}{d t} = - \frac{\bar{c} A_h}{4 V} n_g \qquad (3)$$

and the source density would decrease exponentially with a time constant of $4V/\bar{c}\,A_h$. This value for the OGO-6 mass spectrometer is of the order of 0.02 sec. Physically, this means that the gauge should be emptied of molecules almost immediately if the incoming flux is stopped.

A direct test of the simple model represented by Equation (1) is provided by a comparison of Figures 2a and 2b. Figure 2a is a plot showing typical source density data taken during one orbit of the OGO-6 spacecraft. The observed source densities plotted in Figure 2a were obtained by multiplying the ion current for each constituent by the laboratory sensitivity for that constituent. Figure 2b is an equivalent plot using Equation (1) together with a model atmosphere prediction of ambient densities as a function of altitude.

Atomic oxygen has combined in large part to form molecular oxygen and appears as an ion current at mass 32 and a smaller ion current at mass 16. Both mass 32 and mass 28 have a maximum source density near perigee as expected from the strong dependence of neutral ambient density on altitude. There is, however, an asymmetry in the source density about perigee due to surface absorption processes before perigee and desorption processes after perigee. All the constituents except helium have detectable source densities near apogee as a result of desorption. Finally, the presence of mass 44 (CO_2 or N_2O), mass 1 (atomic hydrogen), as well as carbon monoxide, is thought to result from chemical reactions of atmospheric atomic oxygen with constituents on the instrument surfaces.

Figure 3 shows some long term features of the measured source density data. The perigee and apogee source densities during an orbit are plotted versus time for ions with masses 16, 32 and 28. The perigee density data reflect the changing atmosphere as the spacecraft perigee changes latitude and local time, and as the atmosphere itself varies. The apogee source density is higher than simple theory predicts and depends to some extent on the magnitude of perigee density. It was also found that, after an initial period, the maximum densities for masses 16 and 32 have a nearly constant ratio of 0.1, indicating a common source for these two constituents and a certain stability in the processes leading to these signals. Also, the long term trend in minimum density for mass 28 is decreasing, unlike mass 32, indicating that the processes determining minimum densities are not the same for these two components.

Several problems arose during the operation of the experiment which affect the understanding of the gas surface interactions in the spectrometer. At approximately 30 sec after turnon there was a sudden loss of sensitivity of approximately a factor of 5 (5.03 for mass 32, 4.70 for mass 28, 1.82 for mass 16, 4.32 for mass 4, and 3.46 for mass 2). The exact cause was never determined but was believed to have originated in arcing nearby or within the experiment electronics. No

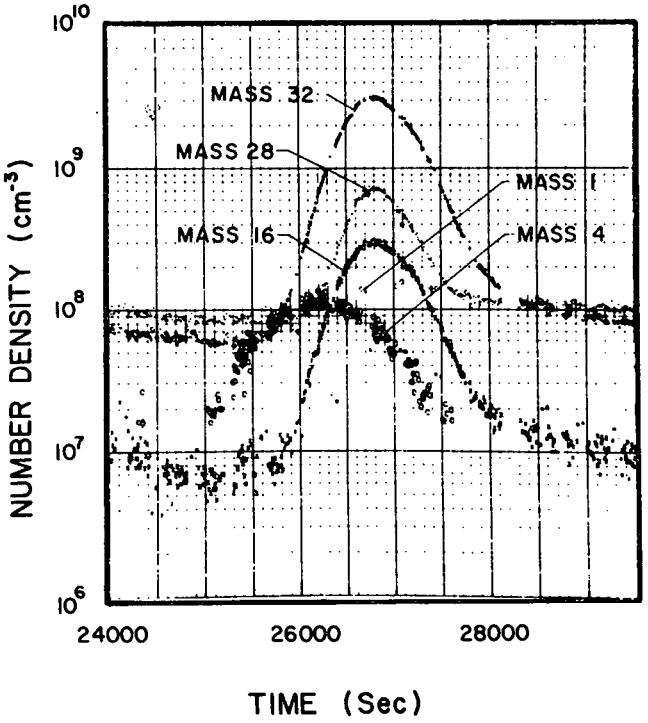

Figure 2a. Observed source densities during a typical orbit for selected constituents. Mass 16 values are due in large part to fractionation of molecular oxygen in the source region.

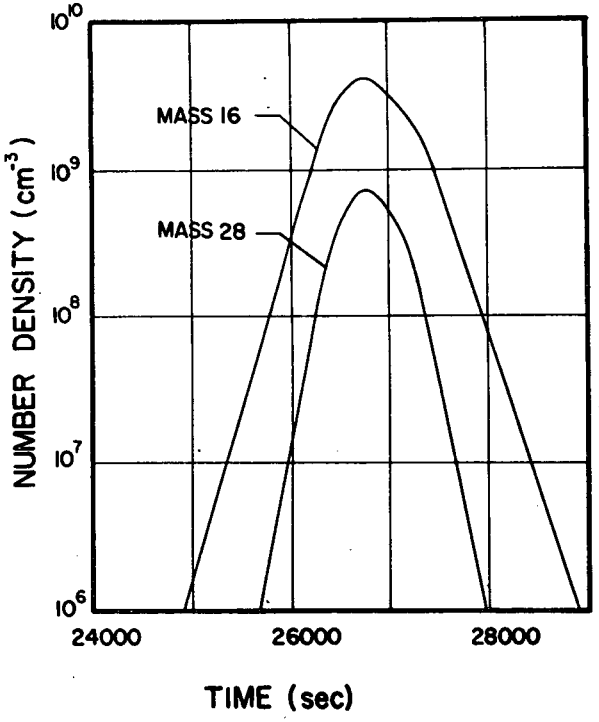

Figure 2b. Hypothetical source densities if there were no gas-surface interactions.

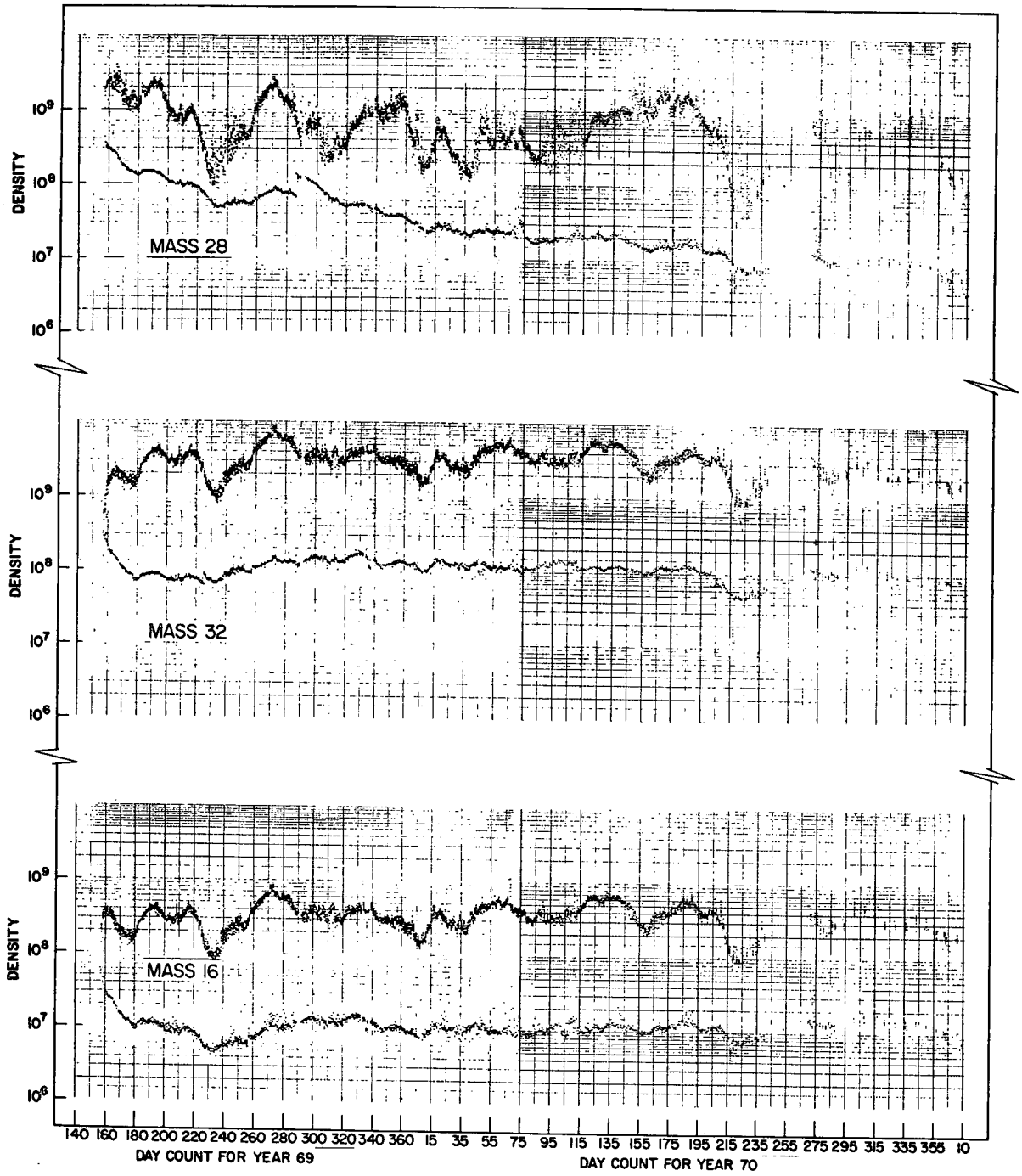

Figure 3. Perigee and apogee source density for constituents with mass 16, 32, and 28.

indication of a further change in sensitivity was found and all densities have been adjusted for this sensitivity change. The change in sensitivity was nearly the same for every mass except 16 and the mass 16 to 32 source density ratio before the shift was near the value expected from fractionation (.0455). Thus it must be assumed that the fractionation ratio of molecular oxygen increased at this instant to 0.16. Later, however, the 16 to 32 ratio is always lower than this value. Despite various laboratory tests on a prototype instrument this failure pattern could not be reproduced and, therefore, the detailed mechanism is not clear. The observation of a constant 16 to 32 ratio after the first two weeks indicates that the new sensitivities have been stable. Nevertheless, the difficulty in determining the correct value to be used for the fractionation pattern of oxygen contributes to the inability to uniquely determine certain surface parameters.

On day 225 of 1969 an electronic failure occurred which put the quadrupole spectrometer into an anomalous operating mode during the measurement of mass 32. The net result was that the ion current recorded for mass 32 became the sum of all ion currents for masses greater than 27. For data acquired after this failure, the mass 28 ion current was subtracted from the mass 32 ion current in the analysis process. Unfortunately, there were some small currents at other masses, particularly masses 30 and 44, which could not be determined with the frequency or accuracy needed to subtract from the measured 32 ion current. The mass 32 source density measurement thus retained a residual contribution from these other masses, as seen by the jump in apogee value at day 225 in Figure 3. The principal effect on ambient density determination is not from the direct contribution, which is negligible near perigee, but in the error it may cause in surface parameter determination.

The temperature of the antechamber is of interest because the surface desorption rate is an exponential function of temperature [Ehrlich, 1959]. A thermistor, located near the source region (Figure 1), recorded changes in temperature of ±10°C with a nominal value of 20°C. These temperature variations are sufficiently large to produce noticeable changes in desorption (nearly a factor of four for a desorption energy of 22 kilocalories/mole). However, the measured temperature may not accurately reflect the effective antechamber temperature because, for example, the measured temperature minimized when the angle between the sun and the front of the antechamber was smallest and this is opposite to the anticipated behavior. The measured temperature was ignored in the final surface analysis, but the data was examined for possible examples of thermal effects.

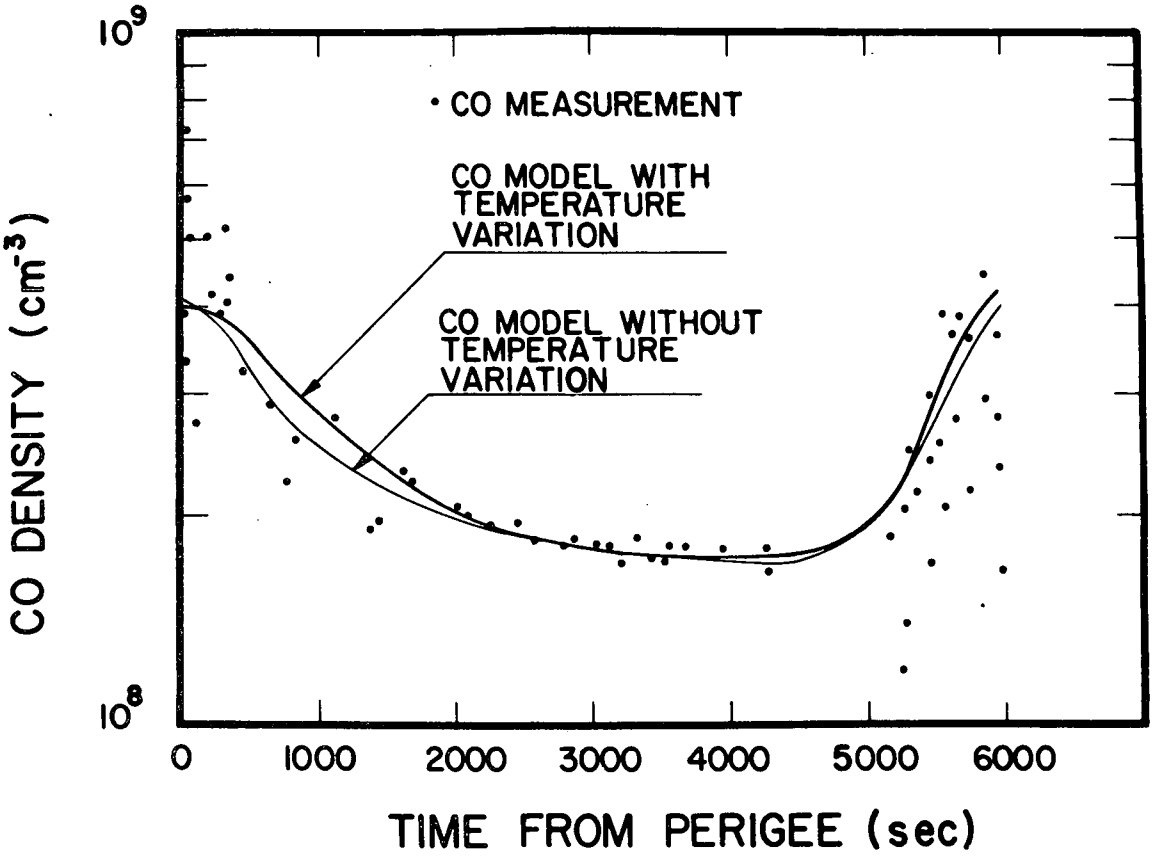

Figure 4. Direct measure of CO during a typical early orbit compared with model estimates. One curve included measured antechamber temperature, the other was computed from a constant temperature model.

N_2 DENSITY

Analysis of gas-surface interactions affecting the mass 28 source density depends critically upon whether the ion current at mass 28 is due primarily to N_2 or CO. If the mass 28 ion current is entirely due to N_2, then we could use an adsorption model for N_2 of the type which has been discussed by Moe and Moe (1967, 1969) in connection with the analysis of pressure gauge data. The net result will be an additive correction before perigee and a subtractive correction after perigee. If, on the other hand, the mass 28 ion current at apogee is due primarily to CO, we must consider the adsorption-desorption reactions of this gas rather than N_2, and the correction will always be subtractive.

The most direct determination of apogee 28 peak composition would come, in principle, from comparing the mass 14 and mass 28 ion currents. Mass 14 ion current results from dissociative ionization of N_2, mass 28 ion current results from both N_2 and CO. Early in the spacecraft's lifetime, the ion current measured at mass 14 indicated that CO was present near perigee. Also during this early period there were substantial ion currents at mass 44, indicating the probable presence of neutral CO_2. Unfortunately, at high altitudes where the concentration of N_2 in the atmosphere is negligible, the ion current at mass 14 is too small to identify the neutral constituent contributing to the mass 28 ion current. The drop in sensitivity referred to earlier resulted in a generally undetectable mass 14 ion current at apogee after the first few days. If the apogee mass 28 ion current were entirely due to N_2, the expected mass 14 ion current would have produced only one or two bits of telemetry signal.

However, the identification of the mass 28 background gas as CO is supported by other evidence. Laboratory experience indicates that CO is almost always present to some degree in evacuated systems. The long term downward trend in the apogee mass 28 source density is not compatible with the apogee density resulting from N_2 desorption unless an ad hoc change in the desorption rate coefficient is postulated. Furthermore, there was a definite, measurable increase in CO at filament change on day 286 of 1969, thus indicating the continuing importance of CO. Finally, previous laboratory work on surface interactions (Trapnell, 1953) indicates that gold is the least reactive of all metals and N_2 the least reactive molecule (except for the noble gases) on any metal, whereas CO is known to chemisorb on gold.

In order to develop a definite model, let us suppose that there exists an initial surface density of carbon which is slowly replaced by diffusion as it is depleted by reaction with O atoms. The base metal, stainless steel, would be a reservoir for carbon which could slowly diffuse through the base metal and the gold-over-nickel surface layer. Extrapolation of available data indicates that the total CO

generated in the instrument will consume a number of carbon atoms equivalent to at least a few ppm of the antechamber base metal.

We assume that CO is produced by two reactions:

$$C\ (wall) + O\ (gas) \rightarrow CO\ (gas)$$

$$C\ (wall) + O\ (wall) \rightarrow CO\ (wall)$$

We further assume that CO is destroyed by three reactions:

$$CO\ (wall) + O\ (gas) \rightarrow CO_2\ (gas)$$

$$CO\ (gas) + O\ (wall) \rightarrow CO_2\ (gas)$$

$$CO\ (wall) + O\ (wall) \rightarrow CO_2\ (gas)$$

Although these reactions represent negligible sinks for O atoms (after the first 20 days of flight) they do constitute a significant loss of CO.

In writing these equations it is assumed that some of the incoming oxygen atoms are adsorbed on the walls. We also distinguish molecules (or atoms) on the wall as a separate species (e.g., CO (wall)) from the ordinary, or gas phase molecules or atoms (e.g., CO (gas)). We have assumed that there are at most two adsorbed states of carbon monoxide and a single adsorbed state of atomic oxygen. It is thought that most chemisorption systems have multiple binding states, each with a distinct sticking coefficient and desorption time constant. It is conceivable, for example, that carbon monoxide adsorbed from the gas phase is bound to the surface mainly in one state and the molecules produced by adatom-adatom combination in a preadsorbed state might be bound primarily in a second state. An attempt to account for this and for the rates of interconversion among the states increases enormously the complexity of the problem. These considerations would be appropriate for laboratory investigations where, in principle at least, conditions may be controlled and are repeatable. We have ignored as far as possible all but the dominant states since we do not have sufficiently detailed information to consider more than one or two surface states.

The following expressions were obtained by considering production, loss, outflow, adsorption, and desorption. In these equations and in those in the following sections we have used k to denote sticking coefficients, σ_{ag} to respresent cross sections for reactions of an adsorbed constituent with one in the gas phase, σ_{aa} to represent a cross section per unit time which describes the rate of reaction of two

adsorbed constituents, and τ_w to represent the lifetime of an adsorbed constituent. A subscript "w" on a density refers to the number per unit area on the wall; a subscript "g" refers to an ordinary volume number density. All of these quantities are associated with a specific process by means of additional subscripts and superscripts, as indicated in Table I.

Outflow is sufficiently rapid that the steady state assumption applies to n_g^{CO}. Consequently,

$$\frac{d\, n_g^{CO}}{d\, t} = \frac{n_g^{16}\, \bar{c}_g^{16}\, n_w^{12}\, A_w}{4\, V}\, \sigma_{ag}^{CO} + \frac{n_w^{CO}\, A_w}{V\, \tau_w^{CO}} - \frac{n_g^{CO}\, \bar{c}_g^{28}}{4\, V}\, (k_{CO}\, A_w + A_h + \sigma_{ga}^{CO_2}\, n_w^{16}\, A_w) = 0 \quad (4)$$

$$\frac{d\, n_w^{CO}}{d\, t} = n_w^{12}\, \sigma_{aa}^{CO}\, n_w^{16} + \frac{k_{CO}\, n_g^{CO}\, \bar{c}_g^{28}}{4} - n_w^{CO} \left(\frac{1}{\tau_w^{CO}} + \sigma_{aa}^{CO_2}\, n_w^{16} + \frac{\sigma_{ag}^{CO_2}\, \bar{c}_g^{16}\, n_g^{16}}{4} \right) \quad (5)$$

Rearranging Equation (4) we obtain

$$n_g^{CO} = \frac{(4\, n_w^{CO}/\tau_w^{CO} + \sigma_{ag}^{CO}\, n_g^{16}\, \bar{c}_g^{16}\, n_w^{12})}{\bar{c}_g^{18}\, (k_{CO}\, A_w + A_h + \sigma_{ga}^{CO_2}\, n_w^{16}\, A_w)}\, A_w \quad (6)$$

assuming dn_g^{CO}/dt is negligible in comparison to the other terms in the equation. If we consider n_g^{16} and n_w^{16} to be explicitly known functions of time, Equation (5) can be solved for n_w^{CO} if n_g^{CO} is replaced by Equation (6). Letting

$$L(t) = 1/\tau_w^{CO} + \sigma_{aa}^{CO_2}\, n_w^{16} + \frac{1}{4}\, \sigma_{ag}^{CO_2}\, \bar{c}_g^{16}\, n_g^{16} - \frac{k_{CO} A_w}{\tau_w^{CO}\, (k_{CO} A_w + A_h + \sigma_{ga}^{CO_2}\, n_w^{16}\, A_w} \quad (7)$$

and

$$Q(t) = n_w^{12} \left\{ \sigma_{aa}^{CO}\, n_w^{16} + \frac{k_{CO}}{4} \left[\frac{n_g^{16}\, \bar{c}_g^{16}\, A_w\, \sigma_{ag}^{CO}}{k_{CO}\, A_w + A_h + \sigma_{ga}^{CO_2}\, n_w^{16}\, A_w} \right] \right\} \quad (8)$$

we have

$$\frac{d\, n_w^{CO}}{d\, t} + n_w^{CO}\, L(t) = Q(t) \quad (9)$$

whose solution is

Table I
Symbol Definitions

A_h = inlet aperture area	(cm^2)
A_w = wall area of antechamber	(cm^2)
$\bar{c}_g^{16}$ = mean thermal speed of atomic oxygen	$(cm\ sec^{-1})$
$\bar{c}_g^{28}$ = mean thermal speed of molecular nitrogen or carbon monoxide	$(cm\ sec^{-1})$
$\bar{c}_g^{32}$ = mean thermal speed of molecular oxygen	$(cm\ sec^{-1})$
$\bar{c}_a^{16}$ = mean thermal speed of ambient atomic oxygen	$(cm\ sec^{-1})$
k_{16} = sticking probability of atomic oxygen	
k_{CO} = sticking probability of carbon monoxide	
n_g^{CO} = density of carbon monoxide in antechamber	(cm^{-3})
n_w^{CO} = density of carbon monoxide on walls	(cm^{-2})
n_g^{16} = density of atomic oxygen in antechamber	(cm^{-3})
n_w^{16} = density of atomic oxygen on walls	(cm^{-2})
n_a^{16} = density of ambient atomic oxygen times ram enhancement factor F(s)	(cm^{-3})
n_w^{12} = density of carbon atoms on walls	(cm^{-2})
n_g^{32} = density of molecular oxygen in antechamber	(cm^{-3})
V = antechamber volume	(cm^3)
σ_{ag}^{32} = adatom-gas atom recombination coefficient	(cm^2)
σ_{aa}^{32} = adatom-adatom recombination coefficient	$(cm^2\ sec^{-1})$
σ_{ag}^{CO} = coefficient of CO production by C (wall) + O (gas)	(cm^2)
σ_{aa}^{CO} = coefficient of CO production by C (wall) + O (wall)	$(cm^2\ sec^{-1})$
$\sigma_{ag}^{CO_2}$ = coefficient of CO_2 production by CO (wall) + O (gas)	(cm^2)
$\sigma_{ga}^{CO_2}$ = coefficient of CO_2 production by CO (gas) + O (wall)	(cm^2)

Table I—(continued)

$\sigma_{aa}^{CO_2}$ = coefficient of CO_2 production by CO (wall) + O (wall)	($cm^2\ sec^{-1}$)
$1/\tau_w^{16}$ = desorption rate of atomic oxygen	(sec^{-1})
$1/\tau_w^{CO}$ = desorption rate of carbon monoxide	(sec^{-1})

$$n_w^{CO} = e^{-\int_{-\infty}^{t} L(t')dt'} \int_{-\infty}^{t} Q(t') e^{+\int_{-\infty}^{t'} L(t'')dt''} dt' + c\, e^{-\int_{-\infty}^{t} L(t')dt'} \qquad (10)$$

or, after sufficient time,

$$n_w^{CO} = e^{-\int_{-\infty}^{t} L(t')dt'} \int_{-\infty}^{t} Q(t')\, e^{+\int_{-\infty}^{t'} L(t'')dt''} dt' \qquad (11)$$

Using this result, we now have from Equation (6):

$$n_g^{CO} = \frac{\sigma_{ag}^{CO}\, n_g^{16} \bar{C}_g^{16}\, n_w^{12} A_w + \frac{4 A_w}{\tau_w^{CO}} \left[Q * e^{\int_{-\infty}^{t} L(t')dt'} \right]}{\tau_w^{CO}\, \bar{c}_g^{28} \left(k_{CO} A_w + A_h + \sigma_{ga}^{CO_2}\, n_w^{16} A_w \right)} \qquad (12)$$

in which "*" denotes convolution.

In the investigation of CO, using a heuristic approach, it was discovered that the CO density could be approximated by an expression of the form

$$n_g^{CO} \approx a'\, n_g^{32} + \frac{b'}{\tau} \int_{-\infty}^{t} n_g^{32}\, e^{-(t-t')/\tau} \cdot dt' + c \qquad (13)$$

The CO density during an orbit was determined by subtracting the mass 14 source density from the mass 28 source density. The mass 14 source density took into account the fractionation ratio and should have agreed with the mass 28 source density if no CO were present. Also, the mass 28 source density within 1500 sec of apogee was taken to indicate CO density, consistent with the earlier decision on the composition of the apogee mass 28 density. After several months

the mass 14 source density near perigee was consistently higher than the mass 28 source density by about 11.4%. There was no way to determine from the available measurements whether this was due to an error in the fractionation ratio or to a true ambient atomic nitrogen density. It was decided to adjust the fractionation ratio to make the two source densities agree during the later orbits.

Equation (13) can be interpreted in terms of a simplified solution of Equation (12) in which σ_{aa}^{CO}, $\sigma_{aa}^{CO_2}$, $\sigma_{ag}^{CO_2}$, and $\sigma_{ga}^{CO_2}$ are ignored and n_g^{32} is assumed to be a rough measure of n_g^{16}. The resulting solution for n_g^{CO} is given by Equation (14) in which $k'_{CO} = k_{CO} A_w/A_h$, a modified sticking coefficient, and $\tau_w^{CO'} = (1 + k'_{CO}) \tau_w^{CO}$, a modified desorption time constant, and $a = a'(1 + k'_{CO})$, a parameter proportional to n_w^{12}

$$n_g^{CO} \approx a \left[\frac{n_g^{32}}{1 + k'_{CO}} + \frac{k'_{CO}}{1 + k'_{CO}} \frac{1}{\tau_w^{CO'}} \int_{-\infty}^{t} n_g^{32} e^{(t'-t)/\tau_w^{'CO}} \, dt' \right] + c \qquad (14)$$

Only during the first two weeks of flight were there sufficient CO data near perigee to allow a determination of all four unknown parameters. The data were grouped into half-day intervals and parameters, a, k'_{CO}, and c were determined for various fixed values of $\tau_w^{CO'}$. A value of 1500 sec for $\tau_w^{CO'}$ provided the best fit to the data. An example of the type of fit obtained is shown in Figure 4. Since temperature variations over the early orbits were small, it made little difference whether they were included or not. The value of k'_{CO} varied daily as shown in Figure 5. It appeared to level off to a value of about 2.5 by day 180 and was impossible to determine after that. After day 180 both $\tau_w^{'CO}$ and k'_{CO} were held fixed. Parameters "a" and "c" were allowed to vary and now values were determined from all the data in a day.

Thus, after day 180 we assume

$$n_g^{CO} \approx a \left[\frac{n_g^{32}}{3.5} + \frac{2.5}{3.5} \frac{1}{1500} \int_{-\infty}^{t} n_g^{32} e^{-(t-t')/1500} \, dt' \right] + c \qquad (15)$$

It is probable that the parameter "c" in Equations (13) through (15) represents a process with a time constant long compared to the orbital period. That is, "c" is not a true constant, but might represent a quantity which changes very little around an orbit. This leads one to suppose that two surface states might be significant for CO, with "c" representing the slower one and

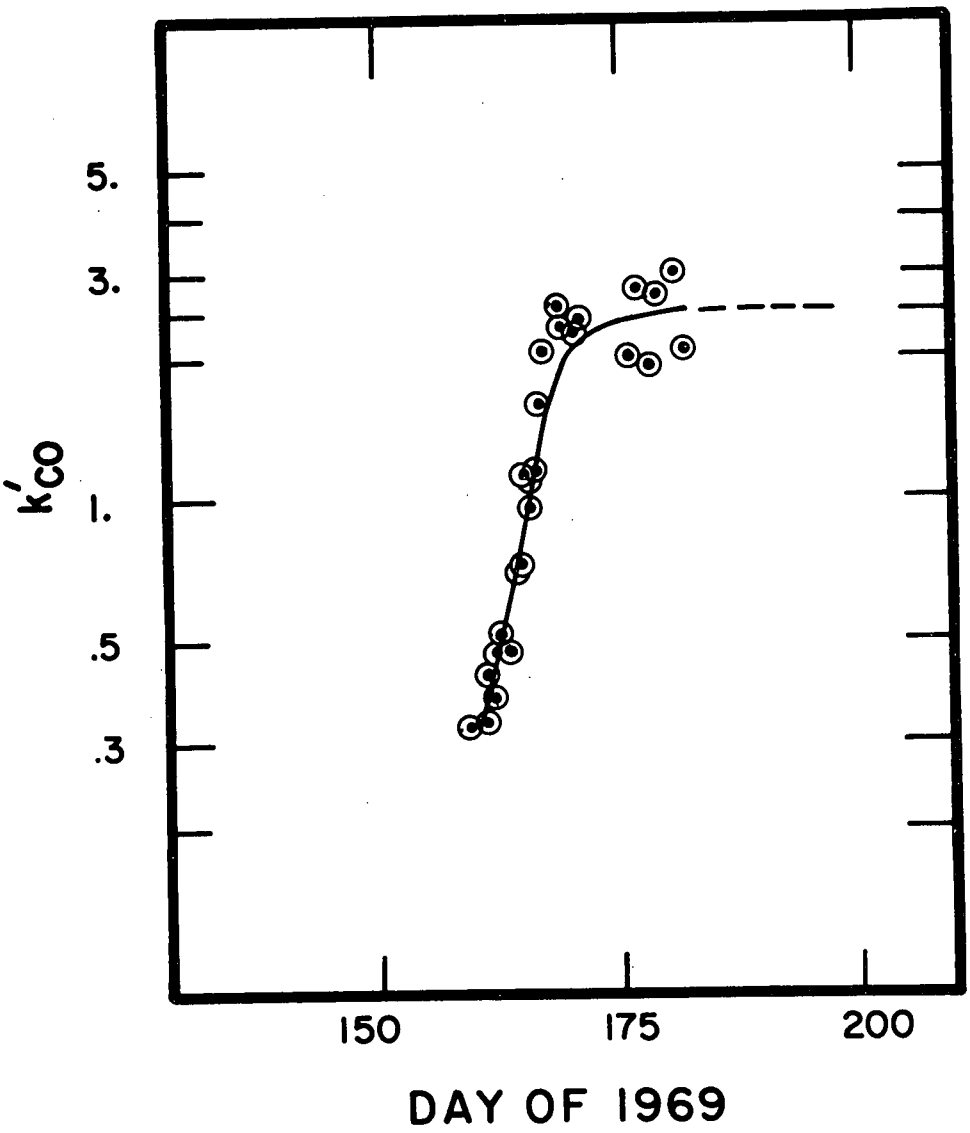

Figure 5. Variation of parameter k' (Equation 14) for the period when CO density was available near perigee. Launch was on day 157.

$$\frac{b'}{\tau} \int_{-\infty}^{t} n_g^{32} \, e^{-(t-t')/\tau} \, dt'$$

the faster one. If this is the case, each surface state must be considered as a separate species governed by its own set of equations having the form of (5), (9), (10), and (11). After the appropriate modifications to (4) and (6), the solution for n_g^{CO} of (12) is replaced by that of (16).

$$n_g^{CO} = \frac{\bar{c}_g^{16} \, n_g^{16} \, n_w^{12} \, A_h \, \sigma_{ag}^{CO} + 4 \, A_w \left[Q * \frac{e^{-\int_{-\infty}^{\tau} L(t')dt'}}{\tau_w^{CO}} + Q' * \frac{e^{-\int_{-\infty}^{t} L'(t')dt'}}{\tau_w'^{CO}} \right]}{[(k_{CO} + k'_{CO}) \, A_w + A_h + \sigma_{ag}^{CO_2} \, n_w^{16} \, A_w]} \quad (16)$$

The symbols Q' and L' refer to the second state and are defined by relations analogous to (7) and (8).

Equation (15) may be regarded as an approximate expansion of (16) in terms of the convenient function n_g^{32}. To the extent that the shape of n_g^{16} resembles n_g^{32}, one may identify the first term of (15) with the first term of (16), the second term of (15) with the second of (16), and so on.

The long term variation of parameter "a" (proportional to the surface wall density of carbon atoms) can be predicted under the assumption this density is diffusion-controlled. If n_w^{12} arose from a diffusion of carbon atoms through the wall of the antechamber, then one expects that n_w^{12} would vary as exp $(-\pi^2 Dt/d^2)$, where d is the wall thickness, D is the diffusion coefficient, and t is time. The diffusion coefficient is not well known but is of the order of 3×10^{-10} cm^2/sec at 300°K (Kittel, 1968).

Figure 6 is a plot of the "a" values for the first six months of spacecraft operation. The curves marked A represent empirical fits to the data points of the form

$$a = a_1 \, e^{-Dy/T_1} + a_2 \, e^{-Dy/T_2} \quad (17)$$

where a_1, a_2, T_1, and T_2 are constants and DY is the day number. Due to the obvious perturbations occurring at the filament change on day 286, a second

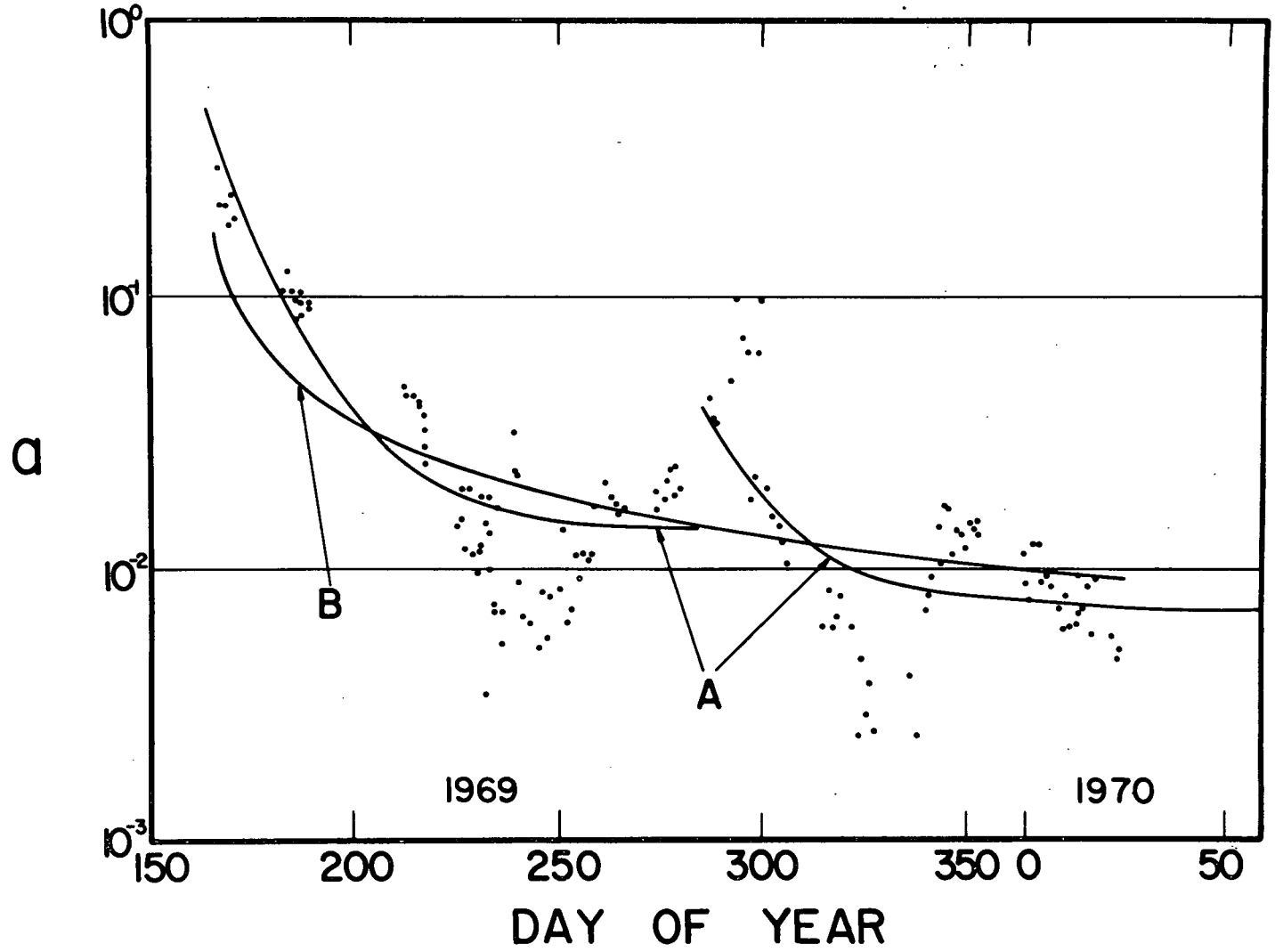

Figure 6. Logarithmic plot of parameter "a" (Equation 15) found from apogee data. If surface carbon density is limited by diffusion through the gold thin film, curve B results. Curves A represent an empirical fit to the data that reflect the ion source filament change in day 287.

curve was used beginning on that day. The B curve has been calculated for comparison, using a diffusion coefficient of 3×10^{-10} cm^2/sec, accounting approximately for the various wall thicknesses of the chamber parts.

The most obvious feature of the "a" vs. time plot (Figure 6) is the cyclic variation of this parameter. This is not consistent with the conception that "a" is proportional to the carbon available for reaction with the incoming oxygen. One expects this parameter to decrease monotonically with time and its profile to have a greater slope when ambient oxygen is highest. Thus, there either must be some explanation for a carbon variation of this form or the apogee slope variation must have a contribution from some source not included in the model. The large excursions of "a" reflect, in part, data analysis problems since "a" was determined primarily from apogee data with a low signal to noise ratio. Also, the excursions might be artifacts of the approximations leading to Equation (16). And, finally, the phenomena in question are extremely temperature-dependent.

The effect of variations in surface desorption rate resulting from variations in surface temperature was studied by recalculating the "a" parameter using temperature as measured by the source thermistor. There was no basic change in the long term variation of "a." Also, individual orbits were examined to clarify the effect of including temperature. A plot of mass 28 source density near apogee is shown in Figure 7a compared with the best fit prediction determined both with and without the temperature variation of desorption. Note that the sign of dn_g/dt can be reversed by including temperature variations. While the data have considerable scatter, the average behavior is better fit by including the temperature variation. On the other hand, Figure 7b shows an orbit where including the temperature variation makes the fit worse. Figure 7c shows the difference over the whole orbit and indicates that there is little practical difference near perigee. The ambiguity of these results may be due to the placement of the thermistor on the outer housing of the antechamber-ion source assembly. Although it gives a general indication of the temperature in the relevant region it is probable that temperature differences of the order of two or three degrees occur, and that at the thermistor the phase of the temperature variation around the orbit might be somewhat different than that inside the antechamber itself.

There is a suggestive correlation between the period of the variation in the "a" parameter and the variations in many spacecraft parameters as a result of the slow (2°/day) drift of the orbit plane with respect to the earth-sun line. If one considers a given point in the orbit, say apogee, the angles between the spectrometer orifice and sun or solar panels and the measured source temperature all have cyclic variations similar to that of the "a" parameter.

One possible way the apogee slope could be modified would be if the spectrometer detected outgassing from the solar panels. Two arguments against this are the

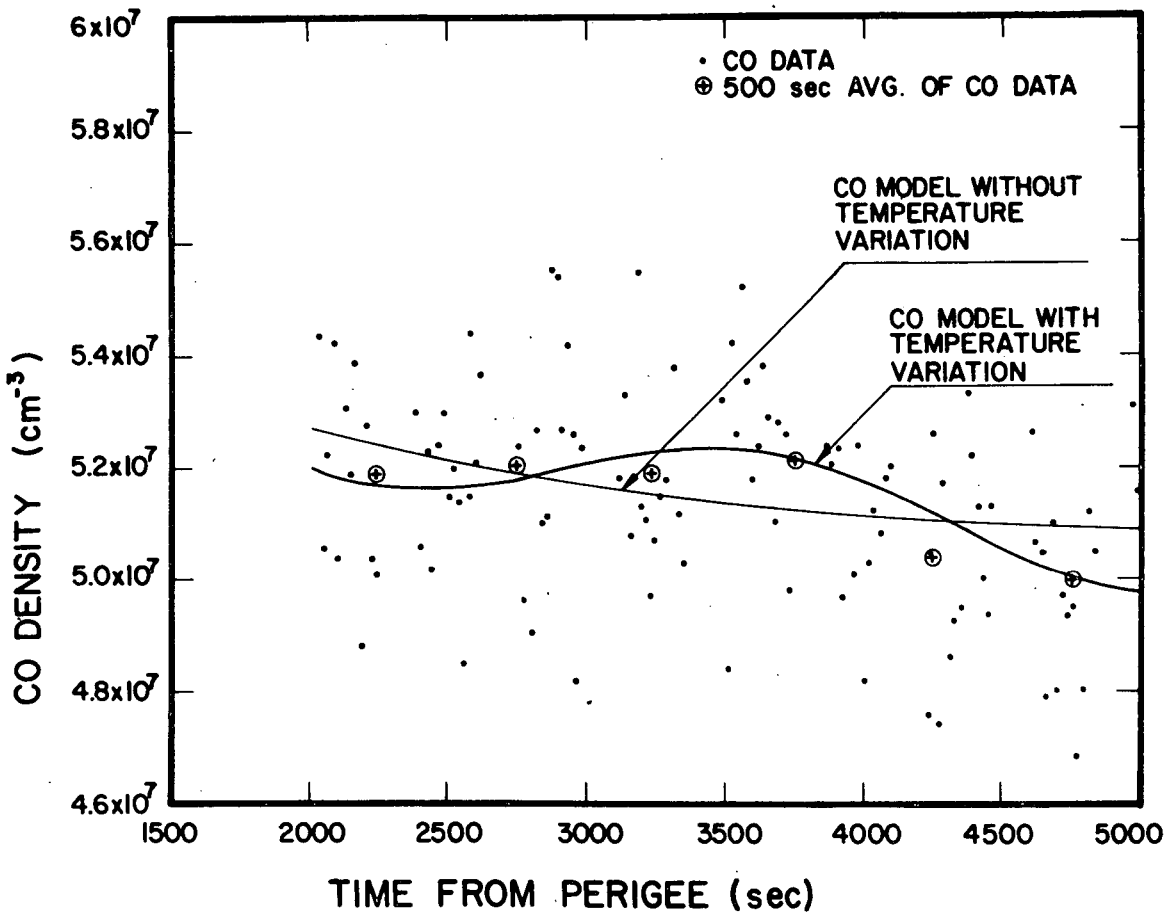

Figure 7a. Comparison of mass 28 source density near apogee with CO density for the same period showing effect of antechamber temperature.

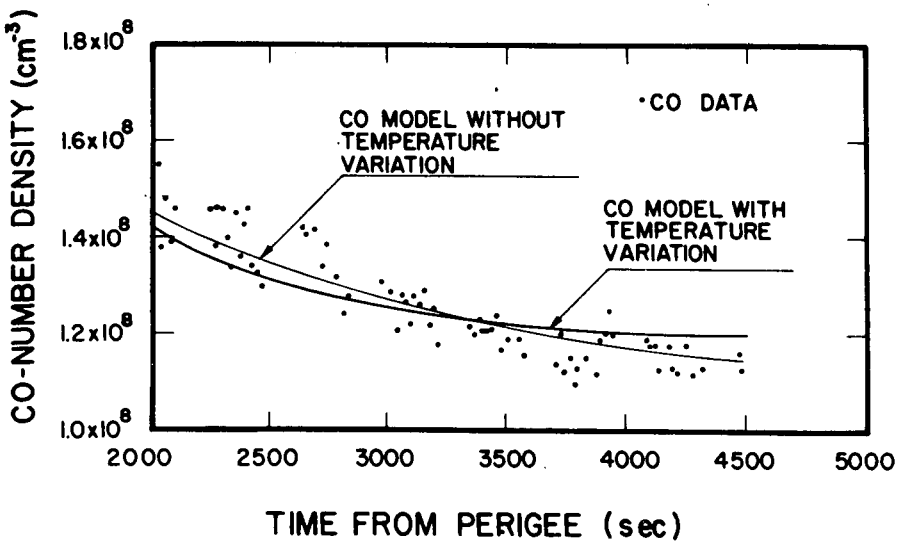

Figure 7b. Same comparison as in (a) for another selected orbit.

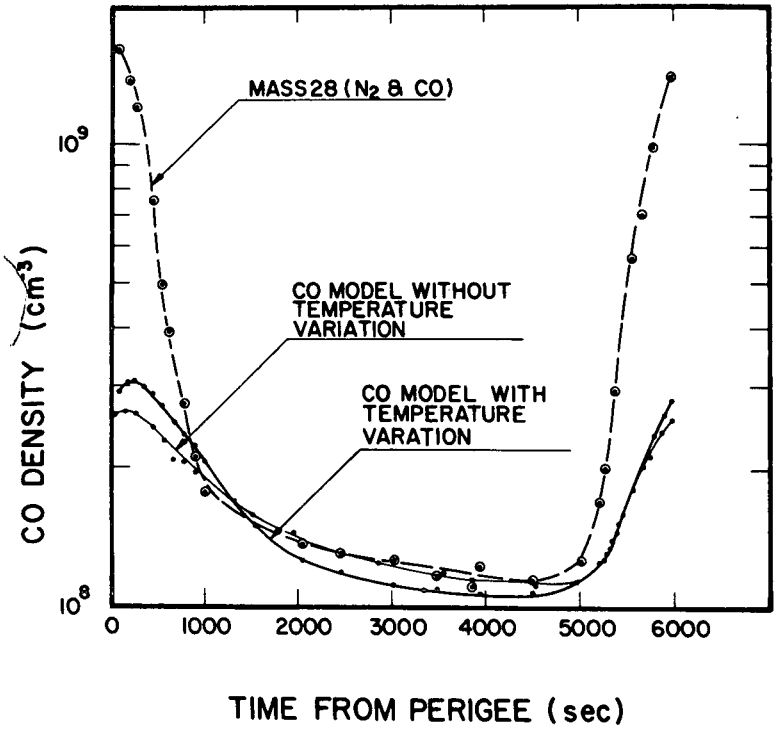

Figure 7c. Comparison of mass 28 source density with CO density for an entire orbit.

lack of detectable variation in the 28 peak at apogee during OPEP scans and the fact that the minimum "a" parameter occurs when the orifice looks at the body before apogee and away from the body after apogee. The latter condition is always associated with noon-midnight orbits.

Figure 8 shows a typical orbit, comparing the observed mass 28 source density with model estimates of the contribution of CO to that source density. Figure 9 shows the fractional error in calculated molecular nitrogen ambient density due to errors in "a" for the data in Figure 8. Note that errors in "a" affect calculated ambient density more severely after perigee and that the calculated ambient density is relatively insensitive to large excursions in "a". This is the inverse of the sensitivity of "a" to errors in the data.

It is clear from Figure 4 that the CO model described is capable of giving a reasonable fit to the measured CO density over an orbit. The problem arises in later orbits when CO density near perigee becomes small, with large errors, and only the apogee density can be used in determining parameters of the model. The small perigee CO density means that the correction is likewise small at perigee, but the CO prediction becomes critical at higher altitudes and its accuracy is one of the factors which limits the altitude of reliable N_2 densities. Because of the danger that variations in the "a" parameter may be the result of extraneous effects not included in the model, we decided to draw a smooth curve through the values, as indicated in Figure 6, and to impose a 50% error bar on the CO correction (interpreted as the difference between the predicted CO and the apogee CO) after day 180 of 1969. For the earlier orbits the CO correction was taken to be accurate to 25%. We believe that from the point of view of producing reliable N_2 densities, a reasonable correction for CO can be made with the method described and the use of N_2 densities with large corrections avoided.

ATOMIC OXYGEN DENSITY

A model of the atomic oxygen interactions in the OGO-6 mass spectrometer has been constructed that accounts for the general behavior of the data. The model is a quasi-equilibrium model which ignores density gradients in the antechamber and variations in surface properties. It is applicable only after approximately 20 days of flight when reactions producing CO and CO_2 become an insignificant loss process for oxygen. It is assumed that the flux of particles into the antechamber from the ambient atmosphere is primarily atomic oxygen with an insignificant component of molecular oxygen. The principal processes are expected to be adsorption of atomic oxygen and gas atom-adatom recombination, with a small amount of adatom-adatom recombination (Wood, et al., 1970).

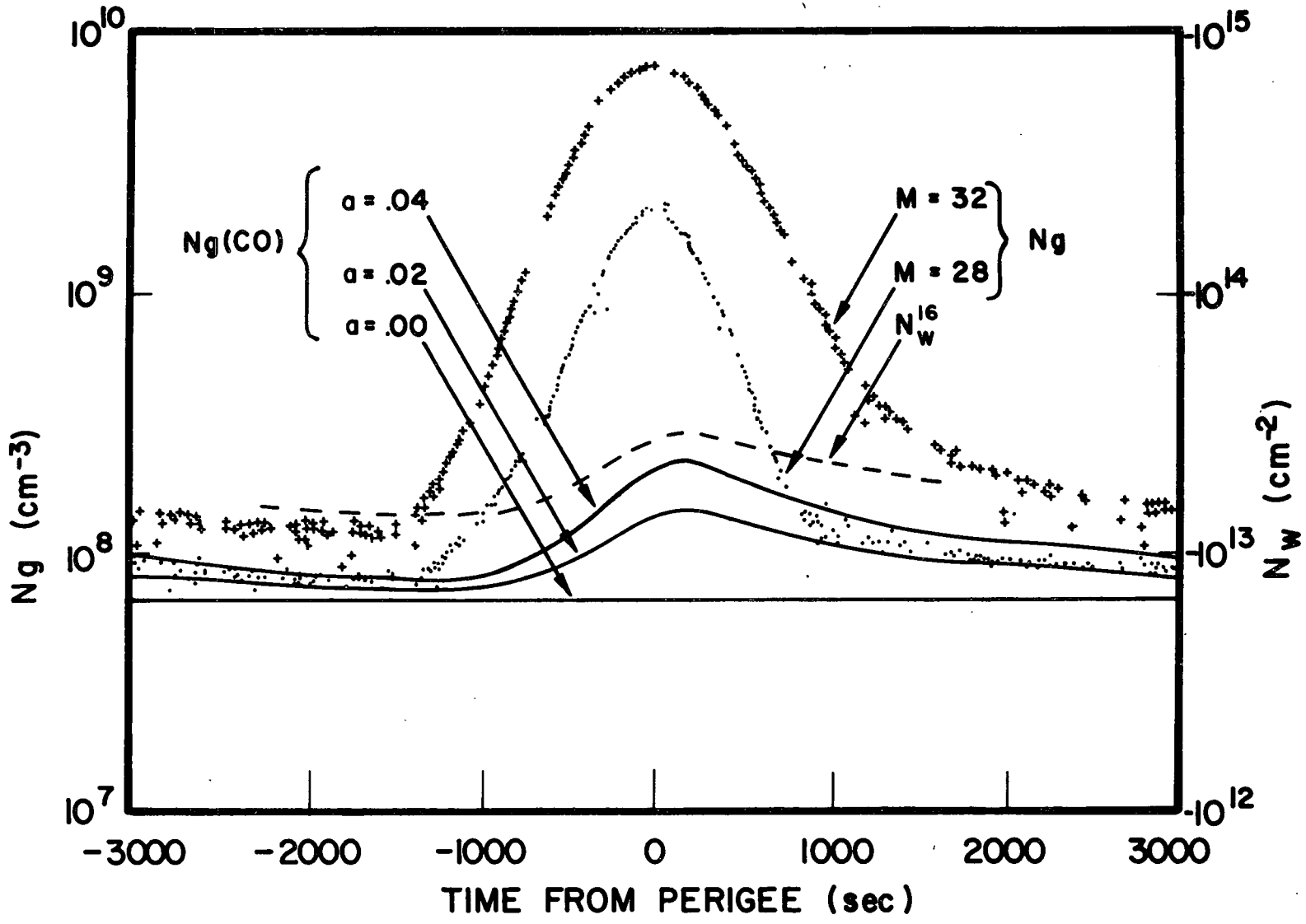

Figure 8. Comparison of mass 28 source density with predicted CO density for several values of "a" (Equation 15). The calculated variation of atomic oxygen wall density for that orbit is shown as well as measured source densities for masses 32 and 28.

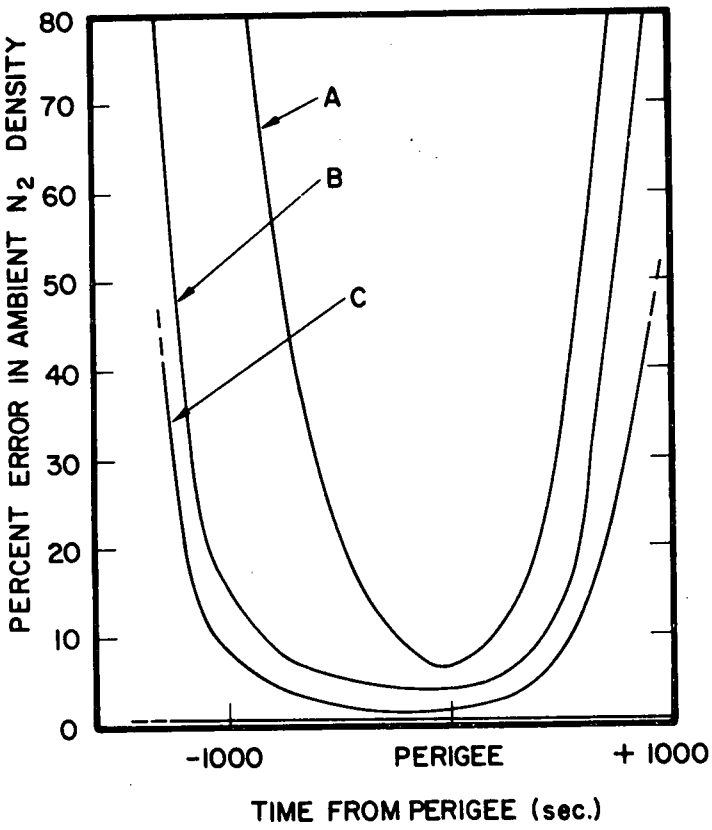

Figure 9. Sensitivity of calculated N_2 ambient density to changes in surface parameters. A: Percent change in ambient density if no surface correction were applied compared with full surface analysis. B: Same as A but correcting for a constant background. C: Density error using a/2 for surface correction compared with the full value "a".

Desorption of atomic oxygen is included to explain the finite atomic oxygen source density at apogee. The interaction of molecular oxygen with the surfaces is ignored, and recombined oxygen assumed to appear immediately in the gas phase, since molecular oxygen is not expected to chemisorb on gold (Trapnell, 1953; Wood, et al., 1970) and would thus have a very short surface interaction time.

The rate of adsorption of atomic oxygen on the antechamber surfaces is proportional to the rate at which gas atoms strike the surface. From elementary kinetic theory, the collision frequency per unit area of a gas with volume number density n_g and mean thermal speed $\bar{c}$ is $n_g\bar{c}/4$. If n represents the number of potential sites (usually taken to be 10^{15} cm^{-2}) and n_w the number of sites that are occupied, then the proportionality constant is $(1 - n_w/n)k$ where k, the sticking coefficient, is regarded as constant (Langmuir Isotherm). It was found that the oxygen surface coverage, using parameters which gave reasonable agreement with the data, was always of the order of 10^{14} cm^{-2} or less and thus the factor $(1 - n_w/n)$ was taken equal to one.

The rate of gas atom-adatom recombination is proportional to the collision rate of gas atoms with the wall and to the number of adsorbed atoms per unit area. The rate of formation of molecules is thus $\sigma_{ag}\, n_g n_w \bar{c}/4$ where σ_{ag} is the recombination coefficient. The rate of adatom-adatom recombination is proportional to the square of the wall coverage, and thus the rate of formation of molecules is given by $\sigma_{aa}(n_w)^2$ where σ_{aa} is the recombination coefficient. The adatom-adatom recombination rate is a function of temperature such that σ_{aa} is proportional to exp (-E/RT) where E is the energy required for surface diffusion and reaction activation, R is the gas constant, and T is the absolute temperature. The desorption of surface atoms occurs at a rate given by n_w/τ where τ is a desorption time constant. The time constant is a function of temperature and is given approximately by $\tau = 10^{-13}$ exp (+Q/RT) where Q is the adsorption energy.

Three equations can be written: one which relates the antechamber density of atomic oxygen to its sources and sinks, one relating molecular oxygen to its sources and sinks, and a similar equation for the wall density of atomic oxygen.

$$V\frac{d\,n_g^{16}}{d\,t} = \left[\frac{n_a^{16}\,\bar{c}_a^{16}\,A_h}{4} - \frac{n_g^{16}\,\bar{c}_g^{16}\,A_h}{4} + \frac{n_w^{16}\,A_w}{\tau_w^{16}} - \frac{\sigma_{ag}^{32}\,n_w^{16}\,A_w\,n_g^{16}\,\bar{c}_g^{16}}{4} - \frac{k_{16}}{4}\,(1 - \sigma_{ag}^{32}\,n_w^{16})\,n_g^{16}\,\bar{c}_g^{16}\,A_w\right] \tag{18}$$

$$V \frac{d n_g^{32}}{d t} = \left[\frac{\sigma_{ag}^{32} n_w^{16} A_w n_g^{16} \bar{c}_g^{16}}{4} + \sigma_{aa}^{32} (n_w^{16})^2 A_w - \frac{n_g^{32} \bar{c}_g^{32} A_n}{4} \right] \tag{19}$$

$$\frac{d n_w^{16}}{d t} = \left[\frac{k_{16} n_g^{16} \bar{c}_g^{16}}{4} (1 - \sigma_{ag}^{32} n_w^{16}) - \frac{\sigma_{ag}^{32} n_w^{16} n_g^{16} \bar{c}_g^{16}}{4} - \frac{n_w^{16}}{\tau_w^{16}} - 2 \sigma_{aa}^{32} (n_w^{16})^2 \right] \tag{20}$$

The symbols are the same as those used in Section 3 and are listed in Table I.

It is now convenient to make the substitutions:

$$\tau_g^{16} = \frac{4 V}{\bar{c}_g^{16} A_h} \approx 0.016; \quad \tau_g^{32} = \frac{4 V}{\bar{c}_g^{32} A_h} \approx 0.023; \quad \tau_a^{16} = \frac{4 V}{\bar{c}_a^{16} A_h}$$

Assuming dn_g^{16}/dt is small with respect to n_g^{16}/τ_g^{16} and dn_g^{32}/dt is small with respect to n_g^{32}/τ_g^{32}, then (18), (19), and (20) can be rearranged and written as

$$\frac{n_a^{16}}{\tau_a^{16}} = \frac{n_g^{16}}{\tau_g^{16}} - \frac{n_w^{16} A_w}{\tau_w^{16} V} + \frac{k_{16} A_w n_g^{16}}{\tau_g^{16} A_h} (1 - \sigma_{ag}^{32} n_w^{16}) + \frac{\sigma_{ag}^{32} n_w^{16} n_g^{16} A_w}{\tau_g^{16} A_h} \tag{21}$$

$$\frac{n_g^{32}}{\tau_g^{32}} = \frac{\sigma_{ag}^{32} n_w^{16} n_g^{16} A_w}{\tau_g^{16} A_h} + \frac{A_w \sigma_{aa}^{32} (n_w^{16})^2}{V} \tag{22}$$

$$\frac{d n_w^{16}}{d t} = \frac{k_{16} V n_g^{16}}{\tau_g^{16} A_h} (1 - \sigma_{ag}^{32} n_w^{16}) - \frac{n_w^{16}}{\tau_w^{16}} - \frac{\sigma_{ag}^{32} n_w^{16} n_g^{16} V}{\tau_g^{16} A_h} - 2 \sigma_{aa}^{32} (n_w^{16})^2 \tag{23}$$

Now if $(-A_h/V)$ times (23) is added to (21) and twice (22) is added to the previous sum, the following general result can be obtained:

$$\frac{n_a^{16}}{\tau_a^{16}} = \frac{n_g^{16}}{\tau_g^{16}} + 2 \frac{n_g^{32}}{\tau_g^{32}} + \frac{A_w}{V} \frac{d n_w^{16}}{d t} \tag{24}$$

The ambient atomic oxygen is the sum of a density derived from the source density of atomic oxygen, twice the source density of molecular oxygen, and a correction which is proportional to the rate of change of the oxygen wall density.

The determination of the wall coverage is found in principle by integrating (23) given the four surface parameters (k_{16}, σ_{ag}^{32}, σ_{aa}^{32}, τ_w^{16}) and values of n_g^{16}. There are three possible sources of n_g^{16} values: (1) directly from the mass 16 source density measurements by subtracting the portion due to the fractionation of molecular oxygen; (2) calculated from (22) using mass 32 source density measurements (n_g^{32}); (3) calculated from (21) using an atmospheric model for n_a^{16}. The first possibility was avoided because n_g^{16} would then be the difference of large numbers and because the fractionation ratio was not known with complete certainty. The second possibility was initially considered the best since it uses the measurements having the least scatter. The third possibility suffers the disadvantage of having to know n_a^{16}, the quantity we are attempting to measure.

An examination of the various equations shows that the surface parameters should, in principle, be determinable from the data. If it is assumed that adatom-gas atom recombination dominates over adatom-adatom recombination near perigee as found by Wood, et al. (1970), we derive from (22)

$$\sigma_{ag}^{32}\, n_w^{16} = \frac{A_h\, \tau_g^{16}\, n_g^{32}}{A_w\, \tau_g^{32}\, n_g^{16}} \tag{25}$$

and this is roughly 0.022. Also near perigee we can see from (23) that k_{16} is roughly equal to $\sigma_{ag}^{32} n_w^{16}$ when σ_{aa}^{32} and $1/\tau_w^{16}$ are small.

The apogee data put further constraints on the parameters. The existence of a finite n_g^{16} implies a finite τ_w^{16} which from (21) is approximately

$$\tau_w^{16} = \frac{\tau_g^{16}\, A_h\, n_w^{16}}{2\, V\, \sigma_{ag}^{32}\, n_w^{16}\, n_g^{16}} \tag{26}$$

assuming n_a^{16} is zero. Assuming also that the apogee mass 32 density is primarily due to adatom-adatom recombination, one can derive from (22) and (24) the values of n_w^{16} at apogee, and σ_{aa}^{32}.

$$n_w^{16} = - \frac{4 V (n_g^{32})^2}{\tau_g^{32} A_w (d n_g^{32}/d t)} \tag{27}$$

$$\sigma_{aa}^{32} = \frac{V n_g^{32}}{A_w \tau_g^{32} (n_w^{16})^2} \tag{28}$$

If it is further assumed that perigee and apogee wall densities are the same order of magnitude, rough values of all the surface parameters will have been determined.

An attempt was then made to refine these approximate values of the surface parameters by a least squares fit of all the mass 16 source densities in an orbit and the mass 32 source densities at apogee. Values of n_g^{16} were predicted from (23) using measured n_g^{32} and values of n_w^{16} calculated from (23). Values of n_g^{32} near apogee were predicted by determining n_g^{16} from (21) with $n_a^{16} = 0$ and substituting it in (22). Equation (23) was solved for n_w^{16} by repeated numerical integration, using values of n_g^{16} calculated from (22), until the n_w^{16} values were the same at the beginning and end of an orbit. While parameters could be found that improved the fit to the data over the rough parameters estimated above, it became apparent that a systematic variation in the residuals (difference between measured and predicted values) was frustrating the search for a satisfactory solution.

The nature of the problem is best seen by examining the ratio of mass 16 to 32 source densities. A plot of these ratios versus time for a whole orbit is shown in Figure 10 which is characteristic of all orbits after the first month. The observed ratio is remarkably symmetric about perigee and has a maximum at perigee. The predicted values of the ratio shown are not the best that can be achieved with a least squares fit, but serve to illustrate the problem. The predicted ratio has a slight dip after perigee and is higher before perigee than after, contrary to the near-perigee behavior of the measured ratio. The reason for the near-perigee behavior of the predicted ratio can be seen from (25). Assuming only that molecular oxygen is the result of adatom-gas atom recombination (independent of how the n_g^{16} level is established) the n_g^{16}/n_g^{32} ratio is inversely proportional to the wall density n_w^{16}. Since the sources contributing to the wall density increase to a maximum near perigee the wall density should likewise increase toward and beyond perigee to reach a maximum where the sources and sinks are equal. This behavior is reflected in the predicted values in Figure 10. A limiting case would exist if the wall density were constant, implying constant n_g^{16}/n_g^{32}. In an attempt to explain the behavior of the oxygen ratio, a number of speculative processes were considered, including: (1) direct surface ionization of wall oxygen in the source; (2) dissociative adsorption of O_2;

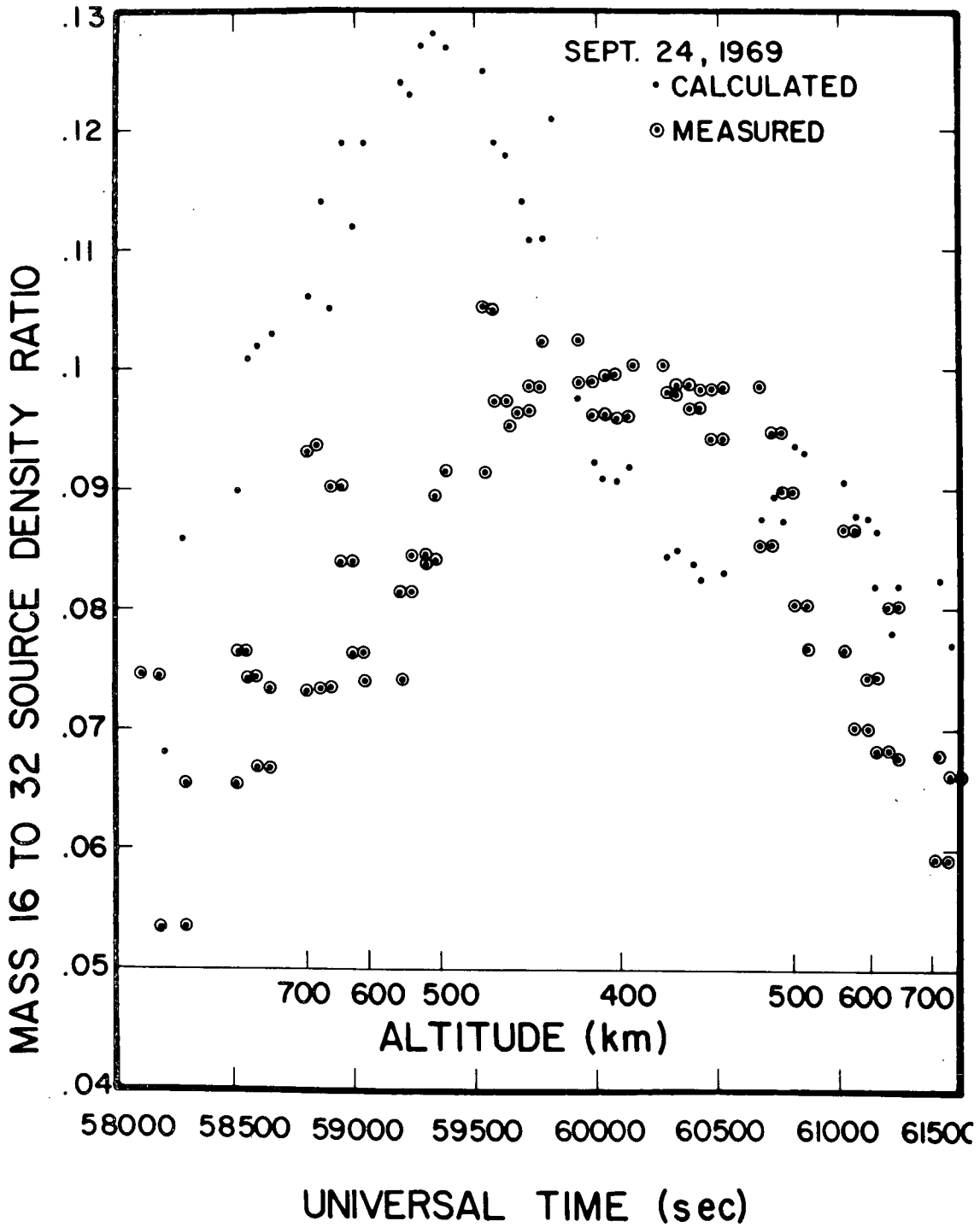

Figure 10. Comparison of measured and calculated 16/32 source density ratios.

and (3) nonhomogeneous distribution of ambient flux on the antechamber walls; but none was satisfactory. A process that would provide maximum n_g^{16}/n_g^{32} at perigee would involve the reaction of O atoms (surface or gas phase) with some other species which peaked at perigee more strongly than O, resulting in a molecule which carries O into the ion source where it is dissociatively ionized. Since neither of these possibilities could be established from the data with certainty or used in a quantitative manner, attempts to fit the data with a method which relied to a large degree on the mass 16 to 32 source density ratio were abandoned.

The method finally used included fitting only the mass 32 source densities over the whole orbit, calculating n_g^{32} from (22) using n_g^{16} from (21) as

$$\frac{n_g^{16}}{\tau_g^{16}} = \frac{n_a^{16}/\tau_a^{16} + n_w^{16}\, A_w/(\tau_w^{16}\, V)}{1 + k_{16}\dfrac{A_w}{A_h}\left(1 - \sigma_{ag}^{32}\, n_w^{16}\right) + \sigma_{ag}^{32}\, n_w^{16}\dfrac{A_w}{A_n}} \tag{29}$$

and obtaining n_w^{16} from (23) as before. Lacking the measured mass 16 source density, the surface parameters cannot be determined without using a model atmosphere for n_a^{16}. Fortunately it can be shown that independent knowledge of all the surface parameters is not necessary to determine the density correction. Only the ratio of k_{16} to σ_{ag}^{32} is important in the correction formula if k_{16} and $\sigma_{ag}^{32} n_w^{16}$ are small with respect to 1. If (22) is solved for n_g^{16} and substituted in (23), the important terms will depend only on the k_{16}/σ_{ag}^{32} ratio. Similarly from (29), with $k_{16} A_w/A_h$ large with respect to 1, the substitution into (23) again produces ratios of k_{16} to σ_{ag}^{32}. Thus it was decided to fix k_{16} at 0.022, which gives rough agreement with the perigee n_g^{16}/n_g^{32} ratio. The value determined by Wood, et al. (1970) was 0.044.

It is also very difficult to separate the two wall loss terms n_w^{16}/τ_w^{16} and $2\,\sigma_{aa}^{32}\,(n_w^{16})^2$ since at apogee, where they are important, the wall density is not changing fast enough to provide a significant difference between linear and square law loss. Thus we decided to fix $1/\tau_w^{16}$ at 6×10^{-5}, which provides an approximate agreement with the apogee mass 16 source density. Numerical experiments showed that within wide ranges the chosen values of k_{16} and τ_w^{16} made no practical difference to the oxygen correction as long as the remaining two parameters were adjusted for best fit to the mass 32 data. We are left with only two surface parameters to be determined: σ_{ag}^{32} and σ_{aa}^{32}.

The model chosen to provide the ambient O densities was basically the static diffusion model of Jacchia (1965), and orbits were selected which, as far as possible, had N_2 densities in reasonable agreement with the mode. This was

accomplished by comparing the exospheric temperature, which yielded the measured N_2 density, with the exospheric temperature predicted by J65. The temperature used for predicting N_2 and O could then be corrected to provide better agreement with the measured N_2. An attempt was made, also, to pick orbits which had perigee near the equator and low magnetic activity. Five orbits were selected for the determination of σ_{ag}^{32} and σ_{aa}^{32}. These occurred on September 22, 24, 26, and November 15 in 1969 and March 22, 1970. The difference between T_n and model temperature T_j is plotted against latitude in Figure 11 along with the modifications actually made to the model temperature when predicting O densities. The predicted O densities were scaled with a multiplicative factor so that only the predicted oxygen latitudinal distribution and not absolute values would be used in determining surface parameters. This factor and the unknown surface parameters were determined by a least squares fit to measured source densities for the selected orbits.

Table II contains values of σ_{ag}^{32} and σ_{aa}^{32} determined for the five selected orbits. Two surface parameters determined from the orbit on September 24 were chosen as the values to be used in ambient density processing because the N_2 densities agreed most closely with the model predictions, because the orbit was during equinox, when cross-equator gradients are least likely, and because the orbital variation of densities indicated that this was an unusually quiet time period (in agreement with the magnetic activity indices). The comparison between the measured and predicted source densities for the September 24 orbit is shown in Figure 12 and the corresponding mass 16 to 32 source density ratio is plotted versus time in Figure 10. The predicted variation in wall density, n^{16}, for this orbit is given in Figure 13.

Rather than calculate ambient densities directly from (29) we decided to assume that n_a^{16} was always zero at apogee and to subtract (24) for the apogee case from (24) for other times giving

Table II
Oxygen Surface Parameters

Date	σ_{aa}^{32}	σ_{ag}^{32}
September 22, 1969	8.67E-19	3.72E-16
September 24, 1969	12.00E-19	3.81E-16
September 26, 1969	4.52E-19	2.80E-16
November 15, 1969	2.20E-19	1.99E-16
March 22, 1970	20.60E-19	4.63E-16

$k_{16} = 0.022 \qquad 1/\tau_w^{16} = 6\ E\text{-}5$

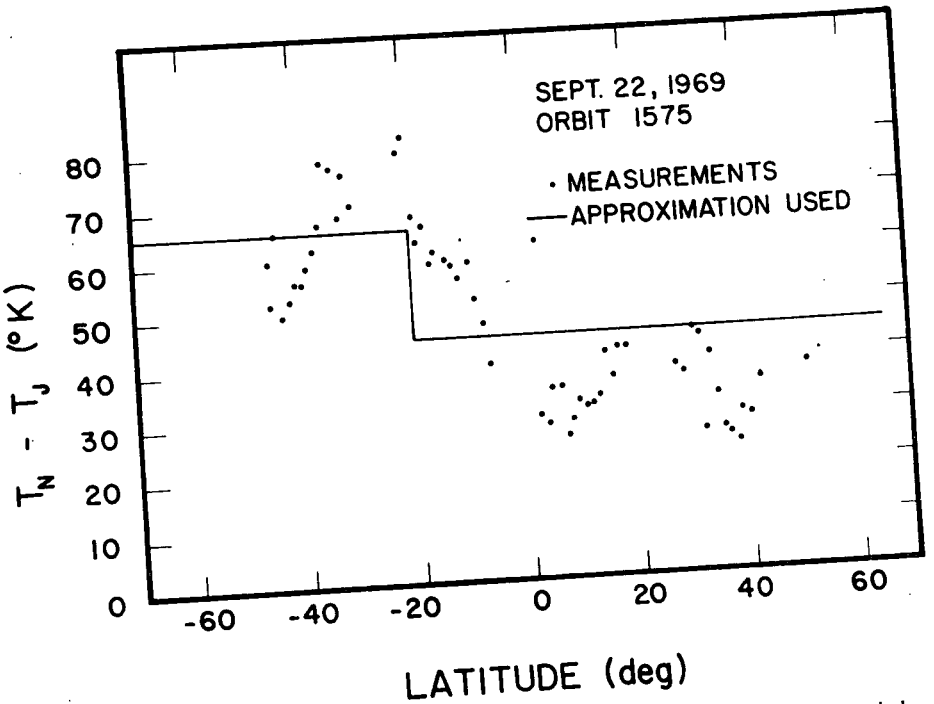

Figure 11a. Comparison of nitrogen ambient density with Jacchia model prediction for orbit on Sept. 22, 1969. T_n is the temperature needed to derive the measured nitrogen density, T_J is the model temperature based on position and geophysical activity. Also shown are the simple approximations used to estimate oxygen surface parameters.

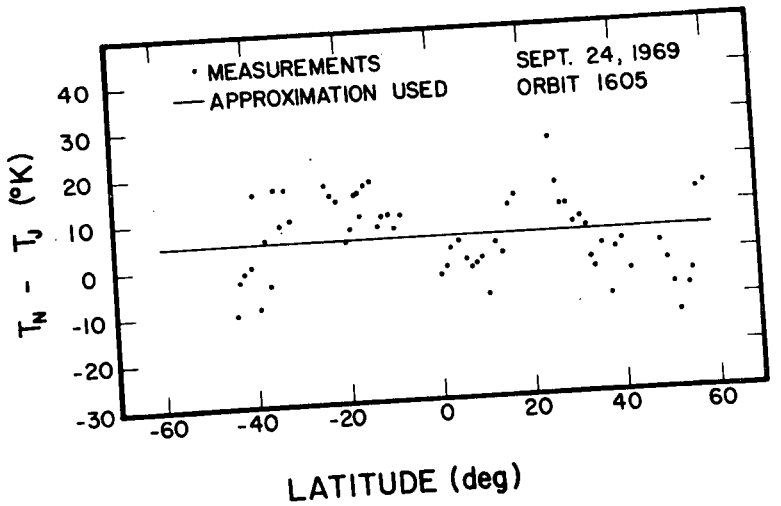

Figure 11b. Comparison for orbit on Sept. 24, 1969.

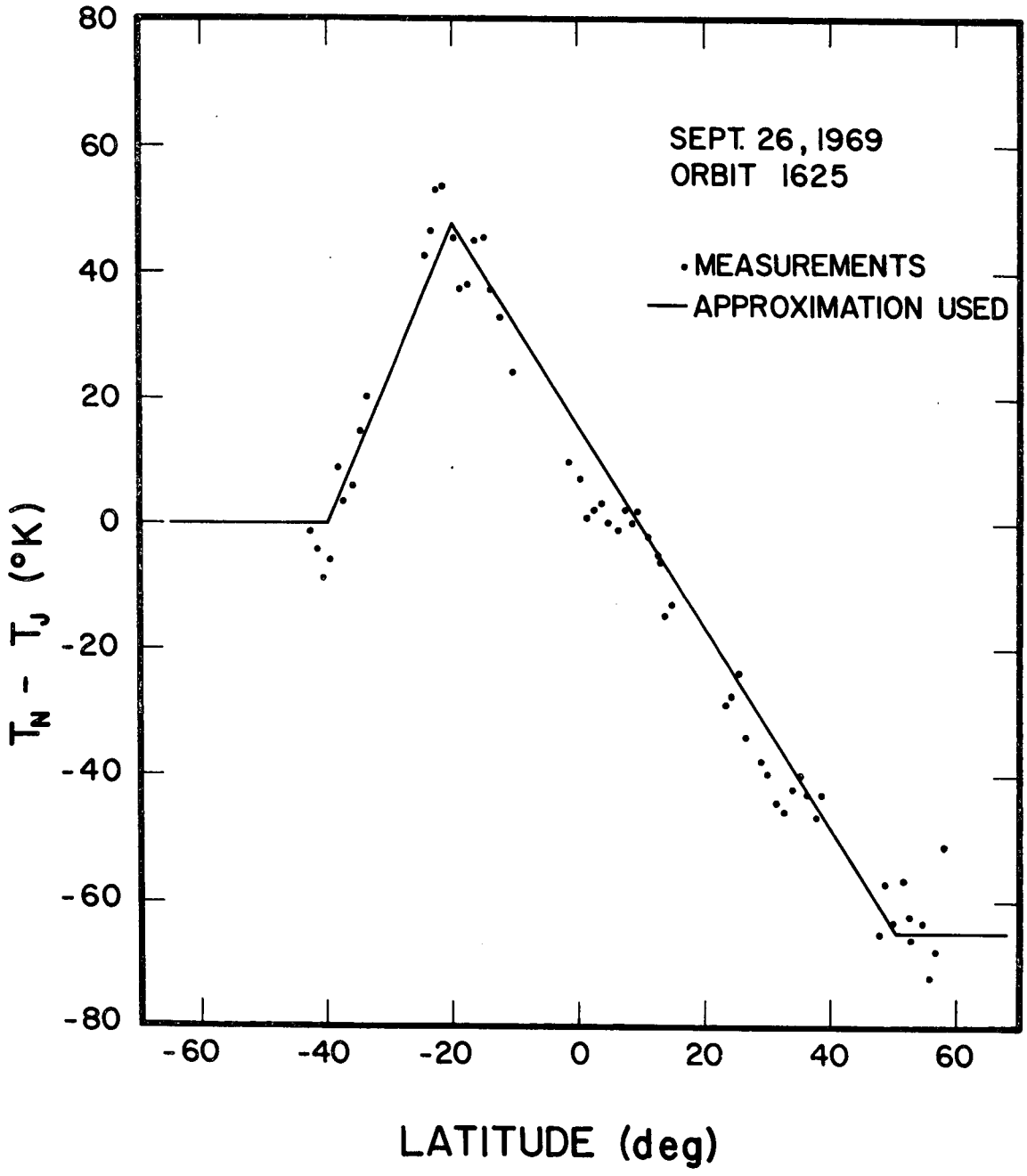

Figure 11c. Comparison for orbit on Sept. 26, 1969.

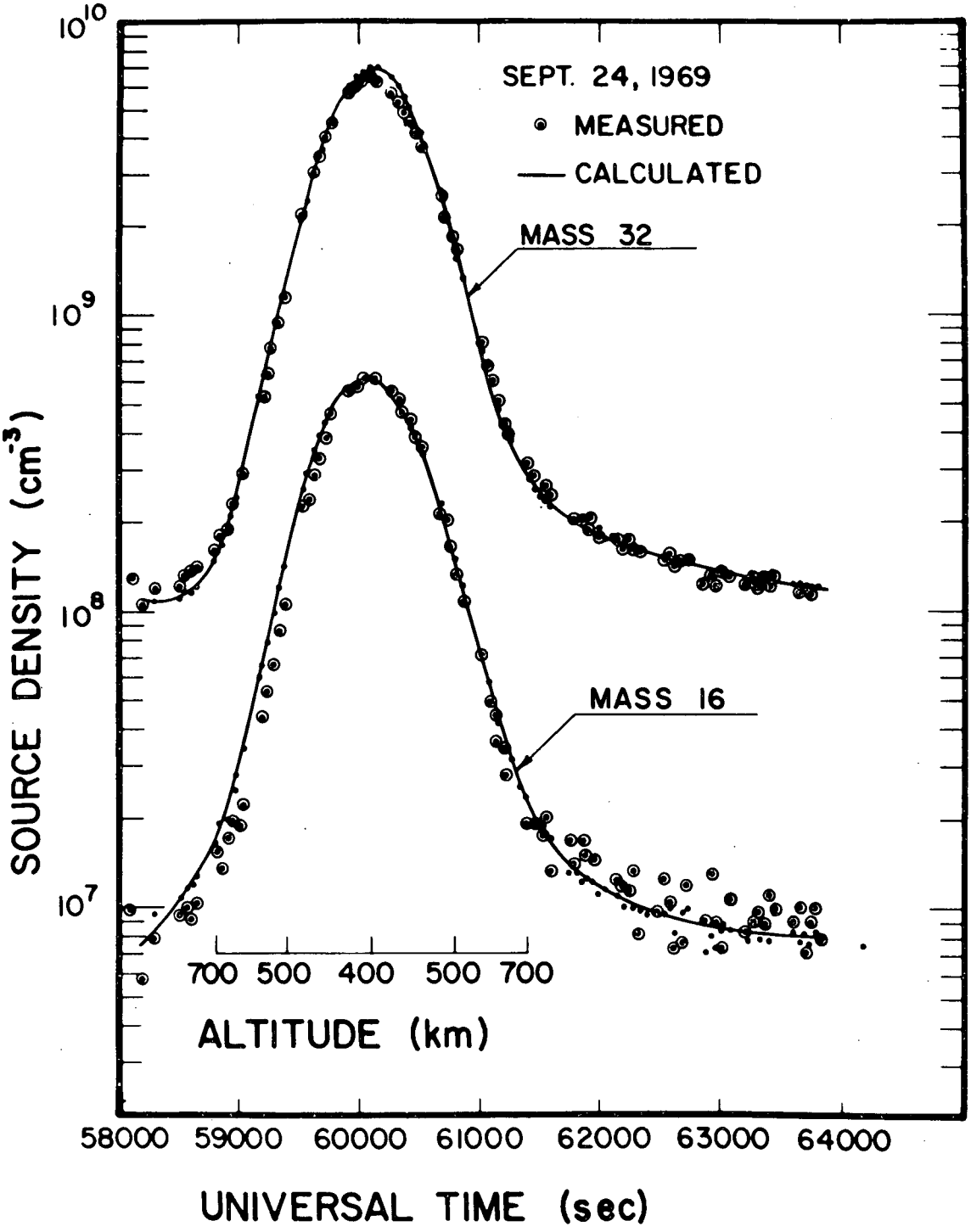

Figure 12. Comparison of measured source density to densities obtained by a least squares fit using Equations 22 and 24.

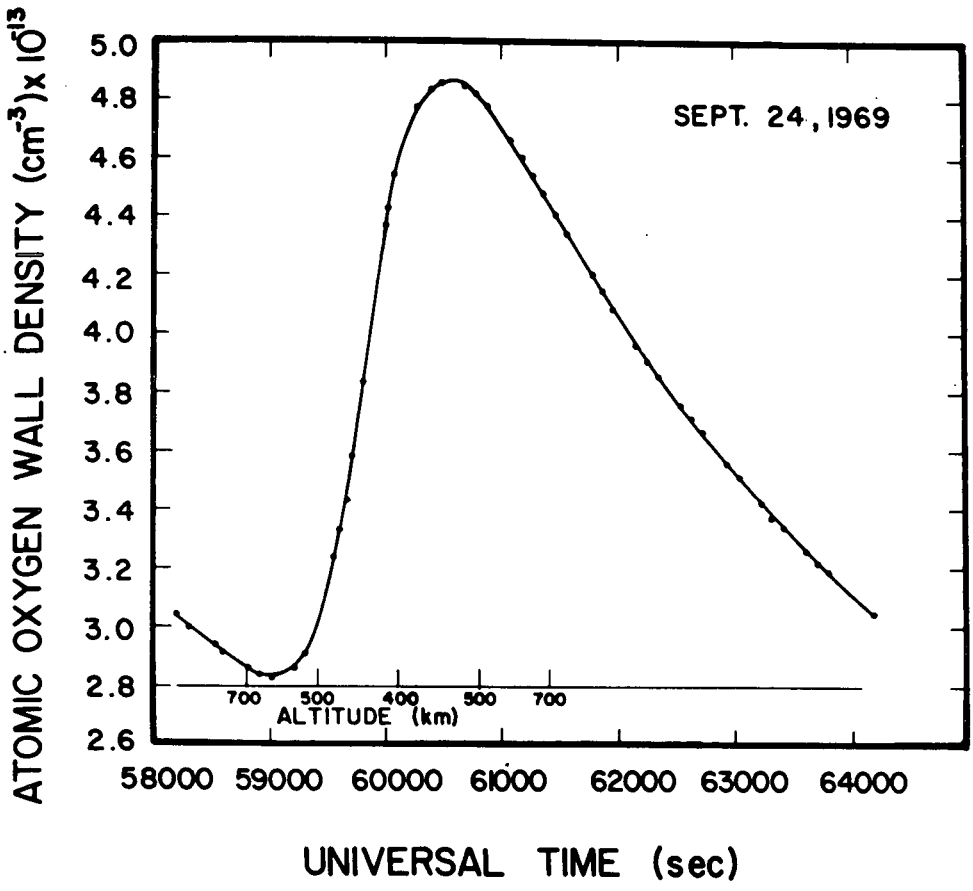

Figure 13. Calculated variation of atomic oxygen wall density for the orbit shown in Figure 12.

$$\frac{n_a^{16}}{\tau_a^{16}} = \frac{n_g^{16} - n_g^{16}\big|_{apogee}}{\tau_g^{16}} + 2\,\frac{n_g^{32} - n_g^{32}\big|_{apogee}}{\tau_g^{32}} + \frac{A_w}{V}\left\{\frac{d\,n_w^{16}}{d\,t} - \frac{d\,n_w^{16}}{d\,t}\bigg|_{apogee}\right\} \quad (30)$$

This has the virtue that the ambient density is assured of tending to zero at apogee regardless of small errors in calculating dn_w^{16}/dt. Perigee results will be essentially unchanged. A correction factor was then defined by

$$CF = \frac{\frac{A_w}{V}\left\{\frac{d\,n_w^{16}}{d\,t} - \frac{d\,n_w^{16}}{d\,t}\bigg|_{apogee}\right\}}{\left(\frac{n_g^{16} - n_g^{16}\big|_{apogee}}{\tau_g^{16}}\right) + 2\left(\frac{n_g^{32} - n_g^{32}\big|_{apogee}}{\tau^{32}}\right)} \quad (31)$$

which means that if ambient densities are calculated by the usual method of ignoring surface effects but subtracting the background (the first two terms of (30)), the densities corrected for surface effects will be (1 + CF) times the density determined from the first two terms of (30). A plot of CF versus time is shown in Figure 14.

The effect of an arbitrary change in surface parameters is demonstrated in Figure 15 by examining the ratio of corrected ambient density to the model ambient density. Note the insensitivity of measured density near 500 km on the outgoing portion of the orbit to changes in surface parameters, which is in agreement with the correction being very low here.

The ambient densities derived for other orbits using the September 24 surface parameters are compared in Figure 16 with the densities derived using the best fit parameters obtained from that particular orbit. There is no large discrepancy except for the November 15 orbit which, being nearer to solstice than equinox, may have composition effects not accounted for in the static diffusion models. The comparison for the March 22 equinox orbit is quite satisfactory. The fact that different pairs of values for σ_{ag}^{32} and σ_{aa}^{32} can give substantially the same ambient densities suggests that there is an effective correlation between the two parameters and this is illustrated in Figure 17 where the line represents sets of parameters for September 24 derived by arbitrarily changing one parameter and least-square-fitting for the remaining one. The parameters for the other days fall very close to this line. This means that with the method used, the surface model has in effect only one degree of freedom.

The extent to which the corrected ambient densities (determined from the measurements depend on the model ambient densities used in determining the surface

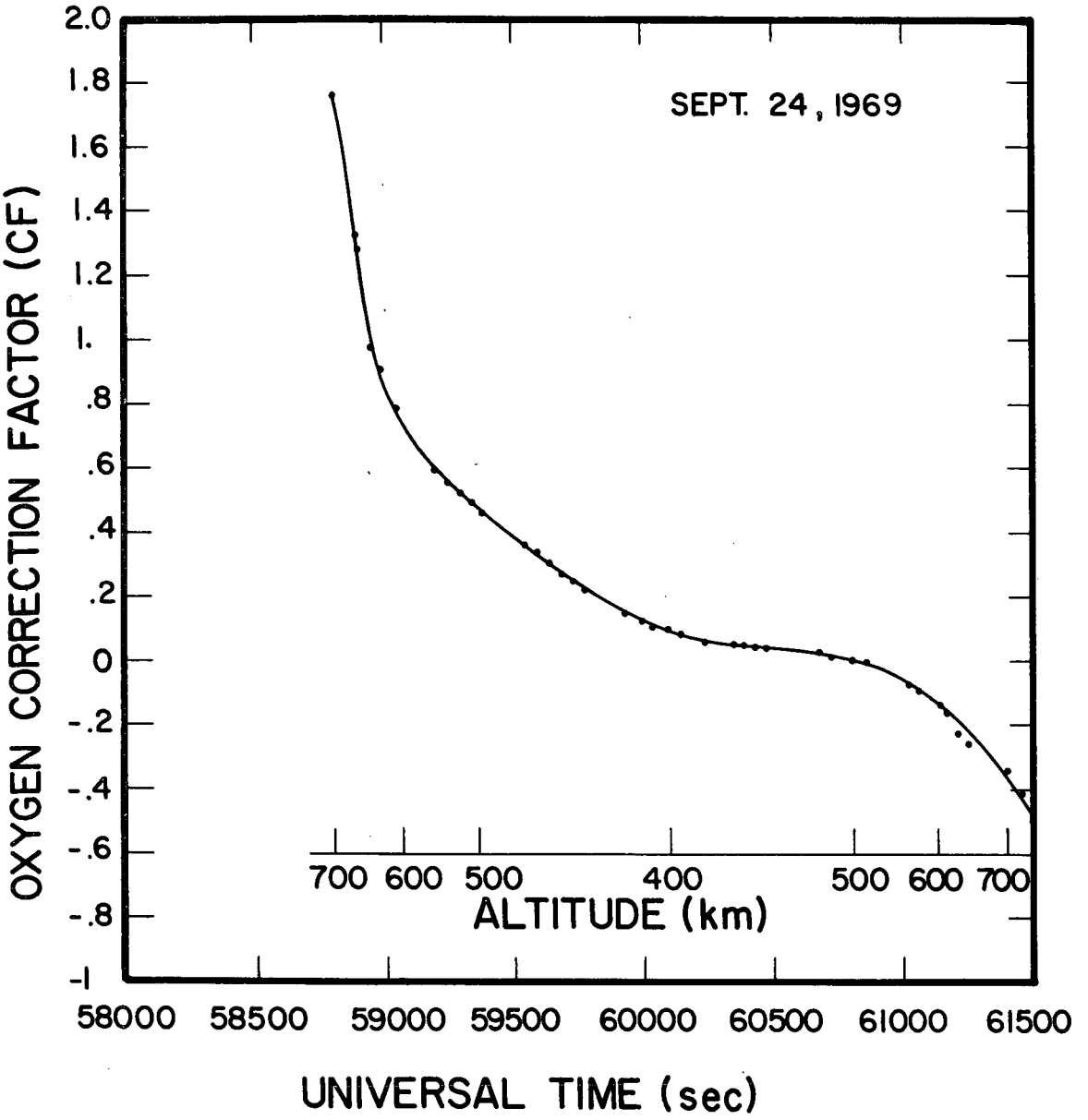

Figure 14. Oxygen correction factor (Equation 31) for the orbit shown in Figure 12.

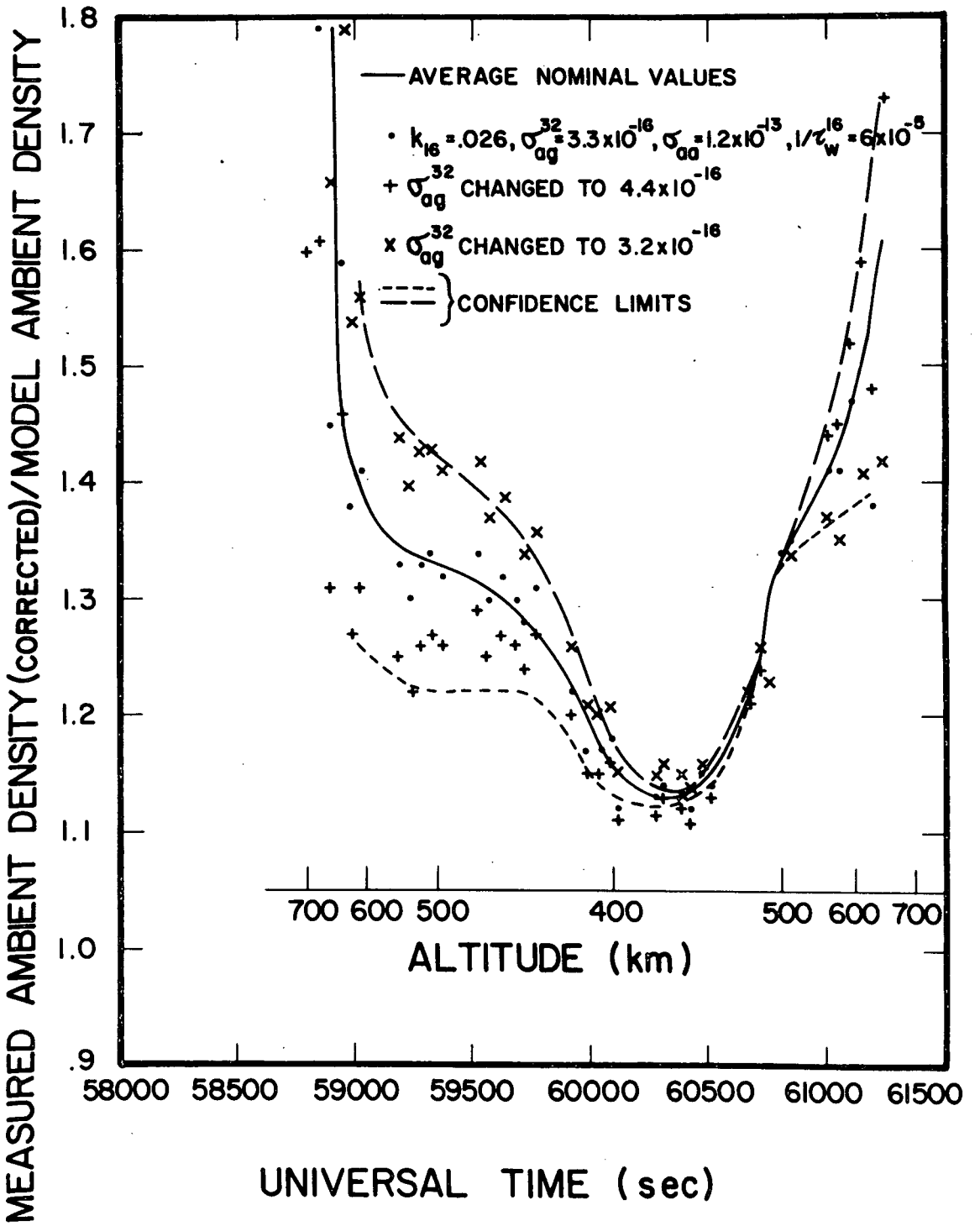

Figure 15. Effect of surface parameter changes on calculated ambient density of atomic oxygen. Also shown are the confidence limits associated with derived ambient densities.

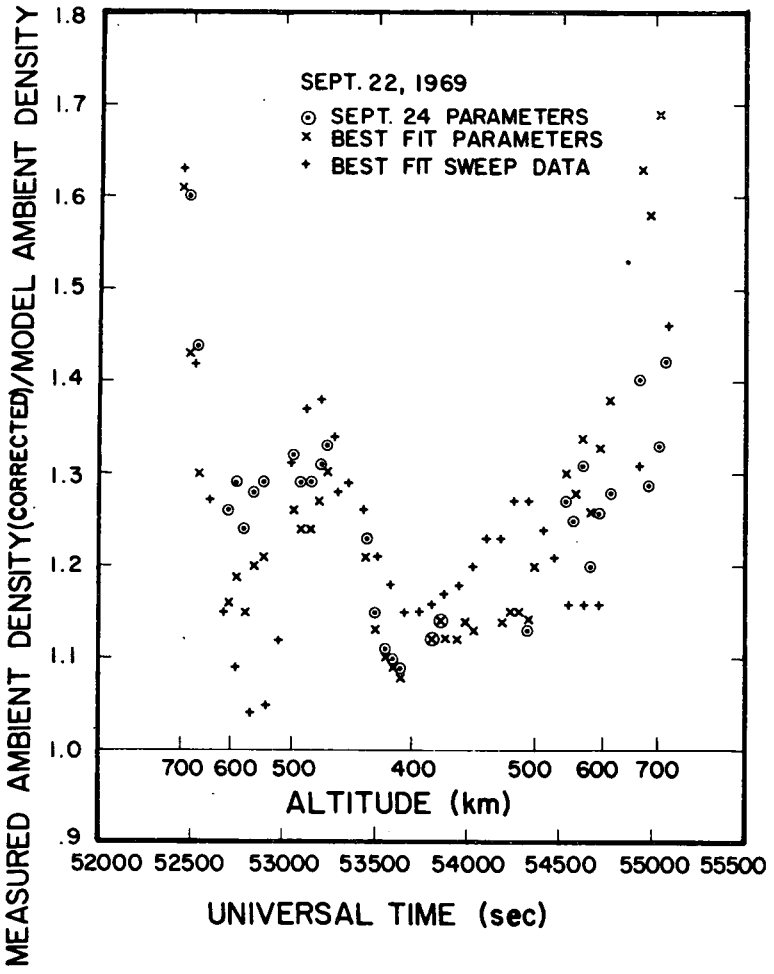

Figure 16a. Comparison of ambient densities derived using Sept. 24 surface parameters and densities derived using best fit surface parameters for orbit on Sept. 22, 1969. An additional comparison is presented using best fit surface parameters from sweep data.

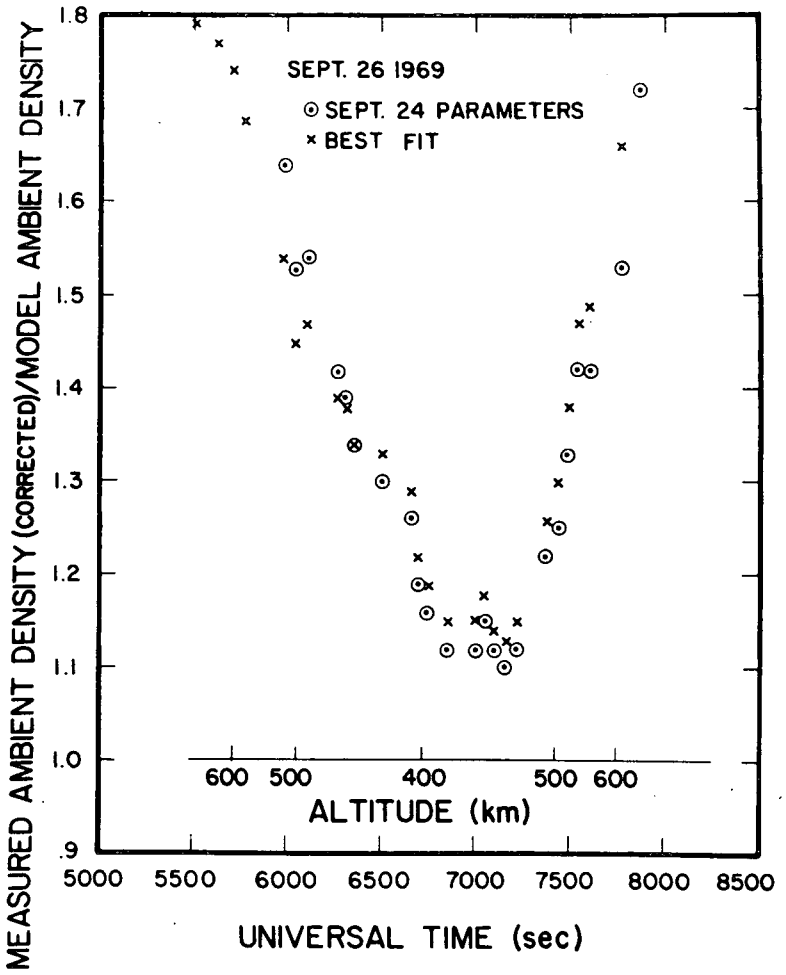

Figure 16b. Comparison for selected orbit on Sept. 26, 1969.

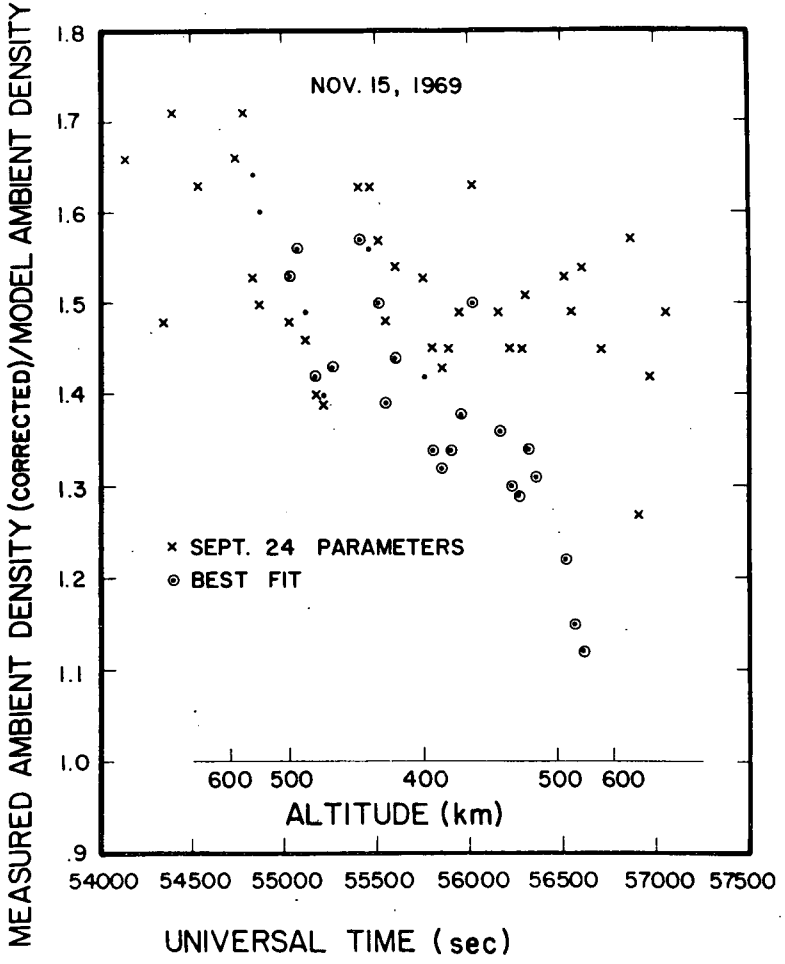

Figure 16c. Comparison for selected orbit on Nov. 15, 1969.

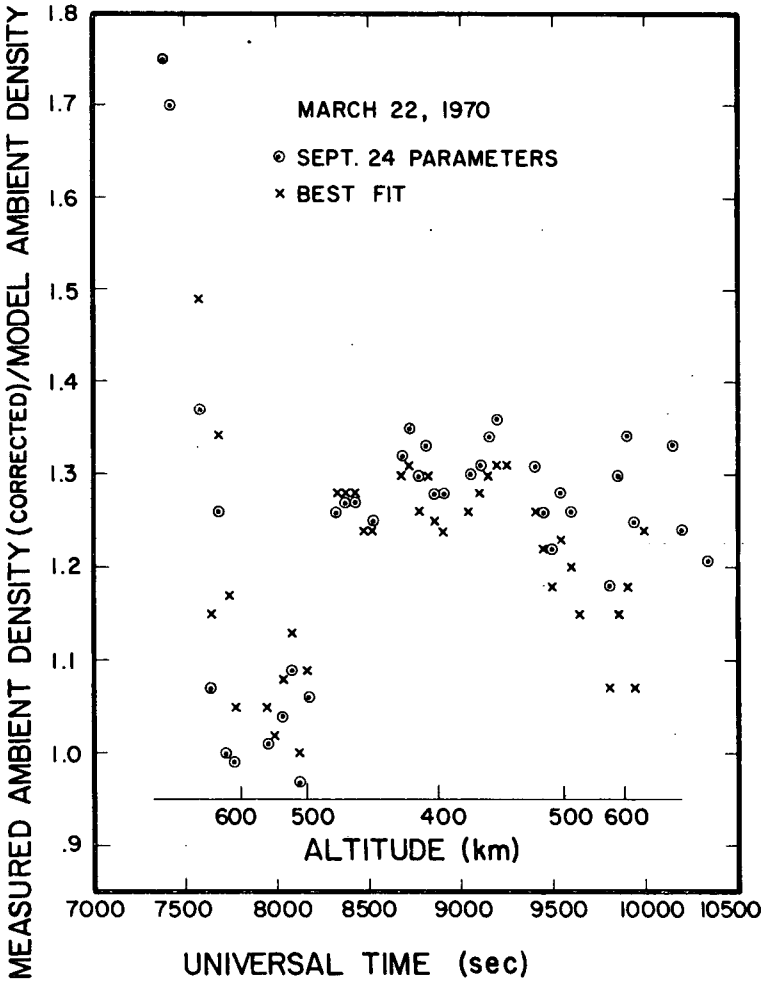

Figure 16d. Comparison for selected orbit on March 22, 1970.

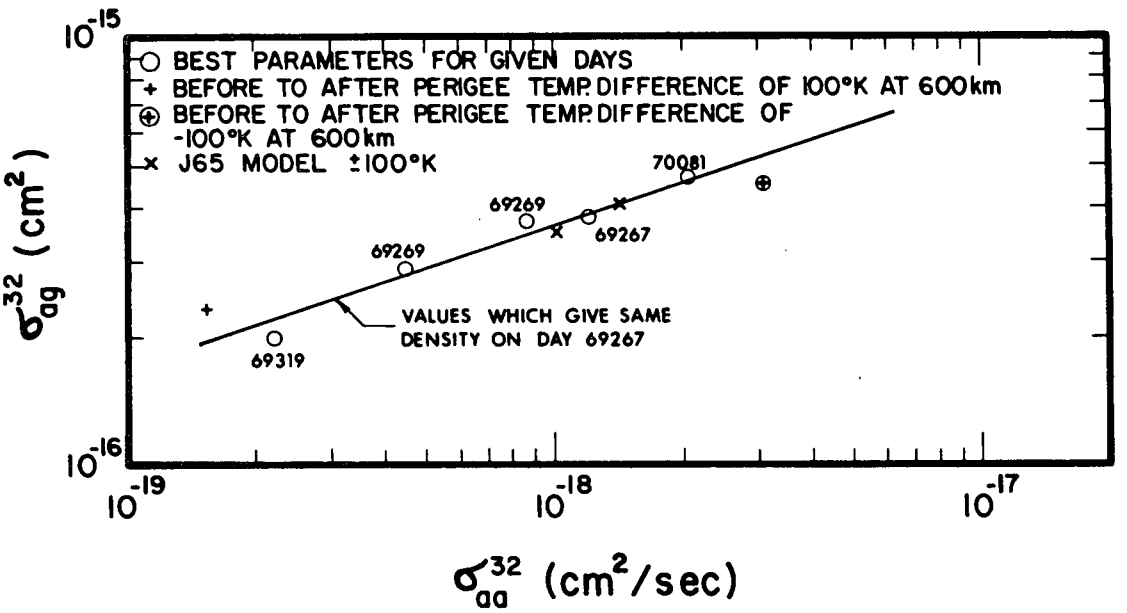

Figure 17. Comparison of derived σ_{ag}^{32} and σ_{aa}^{32} assuming that $k_{16} = 0.022$ and $1/\tau_w^{16} = 6. \times 10^{-5}$.

parameters was studied by making arbitrary changes in the model temperature used to predict the model density. It was found that adding or subtracting a constant temperature to the Jacchia model or using a constant temperature throughout the orbit made no significant difference in the final corrected ambient densities, although the fit to the source density was not always very good and different surface parameters resulted. However, if a temperature gradient of ±1°K per degree latitude was added to Jacchia model temperatures it was found that this gradient was reflected in the corrected density measurements. The same happened for ±2°K but the degree of fit to the source densities was sufficiently poor to suggest that a gradient of this magnitude was unlikely in the real atmosphere for the orbit tested. The result of these tests is that an error in the ambient density model which is symmetric about perigee is unable to cause a significant error in the corrected measured density, but an error in the form of a temperature gradient would be reflected in the measured density.

An assessment of the error resulting from the electronic failure of August 13, 1969, referred to in Section 2, was made by hand-constructing a full orbit curve of mass 32 source density from the sweep mass 32 source density, as opposed to using that obtained in the step mode, and by using this to determine ambient density. Presumably the sweep determinations would be more accurate at the higher altitudes. The densities beyond 600 km using the sweep data were systematically lower than those from the step data. On September 22 the differences were roughly 10% at 600 km and 20% at 700 km (Figure 16a). On September 26 the corresponding differences were 15% and 35%. In addition, the difference between before and after perigee densities at 600 km was about 10% smaller using the sweep data.

During certain time periods (e.g., November 1969) there were changes near apogee in the slope of the source density vs. time plots which suggested that some process in addition to simple desorption was occurring. Maximum deviations in density were on the order of 15%. Three possible explanations were considered: (1) temperature variation of desorption and adatom-adatom recombination; (2) outgassing from the body or solar panels of the spacecraft; or (3) solar radiation entering the spectrometer antechamber. Unfortunately all three possible effects are highly correlated in practice because the normal spacecraft operation was such that when the orifice was facing the sun, the orifice was always facing in the direction of the solar paddles and main body. The phase was such that all three effects could qualitatively predict the perturbations in November 1969, but would not be correct at other times. The ability to predict the temperature effects depends on knowledge of the surface interaction energies, and when these are estimated from the surface parameters already determined, the variations in source density due to temperature appear to be too large. Ambient densities determined by including temperature variations differed from those determined without temperature variations by less than 10% up to 600 km. There

was some evidence for very small variations in source density during OPEP scans which may suggest outgassing from the solar panels or body, but the data are too meager to give quantitative predictions for any time during an orbit.

In summary, a set of surface parameters has been determined which provides a reasonable fit to the mass 16 and 32 source densities and which is consistent with the ambient atomic oxygen predicted by the static diffusion model (Jacchia, 1965) during equinox. It was found that parameters determined from orbits up to 6 months apart were reasonably consistent, which indicates, in conjunction with the constant mass 16 to 32 source density ratio at perigee, that the surface conditions are relatively stable after the first few weeks of flight. The surface model is not applicable to the first few weeks of flight because there was significant production of CO_2 and CO which has not been taken into account.

Unfortunately the surface parameters could not be determined entirely from the source density data, but depended to some degree on an assumed ambient density model. However, the gradient across perigee was the essential feature derived from the ambient density model and we believe that by using an orbit near equinox with perigee near the equator the possible errors were minimized.

During routine processing (23) is solved for n_w^{16} by integrating numerically in serial fashion from orbit to orbit, without the need to repeat the process as was done for a single orbit, and the correction factor (31) is calculated from (24) using the instantaneous n_w^{16}. In order to avoid using ambient densities with large corrections we decided to add to the density error a term equal to 25% of the correction, if positive, and 50%, if negative. The different errors arose because it appeared that a change in a single parameter had twice the effect on the correction when the correction was negative.

REFERENCES

Carignan, G. R. and W. H. Pinkus, OGO-F-04 Experiment Description, Space Physics Research Laboratory, Technical Note 08041-3-T, The University of Michigan, Ann Arbor, October 1968.

Ehrlich, Gert, "Molecular Dissociation and Reconstitution on Solids", J. Chem. Phys., 31, 111, 1959.

Jacchia, L. G., "Static Diffusion Models of the Upper Atmosphere with Empirical Temperature Profiles", Smithson. Contrib. Astrophys., 8, 215, 1965.

Kittel, Charles, Introduction to Solid State Physics, John Wiley & Sons, Inc., New York, 1968.

Moe, Kenneth and Mildred M. Moe, "The Effect of Adsorption on Densities Measured by Orbiting Pressure Gauges", Planet. Space Sci., 15, 1329, 1967.

Moe, Mildred M. and Kenneth Moe, "The Roles of Kinetic Theory znd Gas-Surface Interactions in Measurements of Upper-Atmospheric Density", Planet. Space Sci., 17, 917, 1969.

Silverman, Peter J. and George P. Newton, "Relation of Measured Outgassing Pressures to Surface Adsorption in Satellite Borne Pressure Gauges", J. Vac. Sci. Tech., 7, 323, 1970.

Trapnell, B. M. W., "The Activities of Evaporated Metal Films in Gas Chemisorption", Proc. Roy. Soc., A218, 566, 1953.

von Zahn, U., "Mass Spectrometric Measurements of Atomic Oxygen in the Upper Atmosphere: A Critical Review", J. Geophys. Res., 72, 5933, 1967.

Wood, Bernard J., Bill R. Baker, and Henry Wise, Research Related to Measurements of Atomic Species in the Earth's Upper Atmosphere, Final Report NASr-49(30), Washington, D.C., 1970.